Nonlinear Dyn (2017) 89:1651–1672
DOI 10.1007/s11071-017-3541-y

ORIGINAL PAPER

Analysis of connected vehicle networks using network-based perturbation techniques

Sergei S. Avedisov · Gábor Orosz

Received: 27 September 2016 / Accepted: 21 April 2017 / Published online: 8 May 2017

Abstract In this paper we propose a novel technique to decompose networked systems and use this technique to investigate the dynamics of connected vehicle networks with wireless vehicle-to-vehicle (V2V) communication. We apply modal perturbation analysis to approximate the modes of the perturbed network about the modes of the corresponding cyclically symmetric network. By exploiting the cyclic symmetry, we approximate the dynamics of a given mode by solving a small number of linear algebraic equations. We apply this approach to decompose connected vehicle networks into traveling waves which allows us to assess the impacts of long-range V2V communication on the stability of traffic flow.

Keywords Connected vehicles · Cyclic systems · Perturbation analysis · Modal analysis

1 Introduction

The emergence of wireless vehicle-to-vehicle (V2V) communication has opened up new frontiers in improving traffic flow of ground vehicles. Specifically, it was demonstrated that vehicles using wireless communication may significantly increase highway lane capacity [28]. One of the benefits of V2V communication is the ability of receiving information from multiple vehicles, including those beyond the line of sight [5,15]. Multiple communication strategies may be realized to achieve the desired system level behavior. A commonly studied V2V communication strategy is when each vehicle uses information from the vehicle immediately ahead [13,19,24,25]. In this case wireless communication may be used to control the longitudinal motion of the vehicle, to augment the information obtained by the human operator, or by radar/lidar based sensors. In [2,4,14,31,32] the benefits of developing more generic communication strategies that exploit long-range communications were emphasized. A common V2V-based control strategy is called cooperative adaptive cruise control (CACC) [1,10,16,17,23,27] where each vehicle uses the V2V information sent by a designated vehicles downstream while also monitoring the motion of the vehicle immediately ahead. The CACC strategy was experimentally verified for small platoons of vehicles [10]. However, CACC requires a designated leader and all vehicles must be equipped with sensors and wireless communication. That is, it may be difficult to implement in mixed traffic scenarios where only a few vehicles are equipped with V2V communication.

To improve the smoothness of traffic flow using V2V communication, a modular communication-based control strategy called connected cruise control (CCC)

S. S. Avedisov (✉) · G. Orosz
Department of Mechanical Engineering,
University of Michigan, Ann Arbor, MI 48109, USA
e-mail: avediska@umich.edu

G. Orosz
e-mail: orosz@umich.edu

was put forward in [3,7,9,21,32] that exploits V2V information from multiple vehicles ahead without a pre-defined communication structure. The arising connected vehicle network (CVN) may include CCC vehicles as well as human driven vehicles, which may or may not transmit information. The design of the CVN with CCC vehicles allows one to improve mobility while accounting for the diversity of traffic. On the other hand, allowing such diversity and flexibility requires techniques for continuously gauging the performance of CVN.

To evaluate the performance of CVN we place the vehicles on a circular road. This results in an autonomous system, where one may track traffic waves and perform bifurcation analysis to quantify nonlinear effects [3,6]. Furthermore, when the number of vehicles on the ring road is sufficiently large, the behavior of CVN was shown to be equivalent to that of a chain of vehicles on a straight road [6,8]. To evaluate the effect of CCC vehicles at a system level demands methods that account for the heterogeneity of vehicles and communication strategies of mixed traffic. Such methods shall allow for reduction of the dynamics of large vehicle systems without being computationally demanding.

To simplify the analysis of a network of connected nodes, we first consider a system with simple connectivity structure and then use perturbation theory to analyze networks with more complex connectivity structures. In the literature, perturbation theory was used to analyze the modes of near-cyclic systems dealing with vibrations and localized modes of bladed disk assemblies [11,12,22,30]. In particular, closed-form analytical approximations for the eigenvalues and modes of mistuned bladed disk assemblies were obtained by expanding the equations around the corresponding cyclically symmetric assembly. Such perturbation analysis was more computationally effective compared to a global eigenvalue analysis and also gave insight about the effects of mistuning on the frequencies and mode shapes for simple one-degree-of-freedom mechanical systems with nearest neighbor interactions. Recently, modal perturbation analysis was used in [29] to evaluate the performance of a CVN where each vehicle is modeled by a delay differential equation. The technique allowed the authors to characterize the modal stability boundaries of a network of three connected vehicles on the ring road. However, the analysis did not exploit the cyclic structure of the network and such analysis would become cumbersome (or impossible) for a larger number of vehicles with more complex dynamics and interaction laws.

In this paper we develop a network-based modal analysis technique for perturbed cyclic systems with an arbitrary number of nodes, multiple equations per node and for multiple acyclic perturbations. By exploiting the cyclic structure of the unperturbed system, we use a series of steps to decompose the perturbed cyclic system into decoupled modal equations. Such a modal decomposition can be performed for systems with arbitrary numbers of nodes and an arbitrary number of perturbations without significant increase in complexity. The linear stability conditions can then be evaluated independently for each mode, and the effects of the perturbations on modal stability can be quantified. In addition to being convenient for systems with large numbers of nodes and acyclic perturbations, this technique allows one to determine analytical relationships between system parameters and modal behavior, which would be extremely difficult and cumbersome with traditional analytical and numerical stability analysis. We use the developed technique to examine the linear stability of a CVN consisting of both conventional vehicles and CCC vehicles and analyze how the gain parameter used for the long-range connections shall be selected to stabilize the traffic flow.

The layout of the paper is as follows. The mathematical model for the CVN is given in Sect. 2. A general perturbation method to estimate the modal dynamics of a cyclic system with a general class of acyclic perturbations is presented in Sect. 3. In Sect. 4 we utilize this method to estimate the modal dynamics of CVN, examine the stability of several specific connected vehicle configurations and validate the developed modal perturbation technique using numerical continuation. Finally, we discuss the implications of the results and lay out future research directions in Sect. 5.

2 Modeling connected vehicle networks

In this section we develop a model for connected vehicle networks where vehicles may exploit information from multiple vehicles ahead, see Fig. 1a. We first setup a conventional vehicle network in which each vehicle responds to the vehicle immediately ahead. Then we select a set of vehicles that can broadcast their

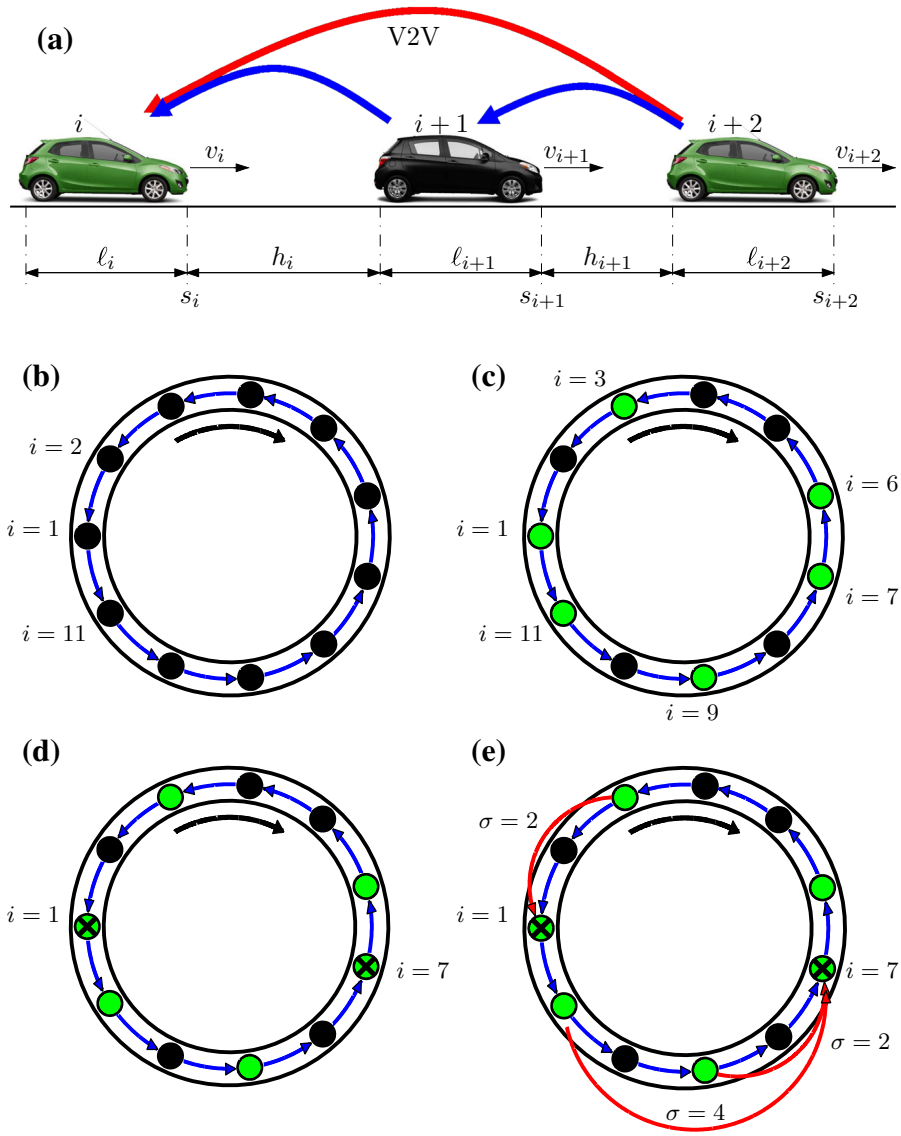

Fig. 1 **a** Side view of connected vehicle network including a transmitting vehicle (*right*) a conventional vehicle (*center*) and a CCC vehicle (*left*). **b–d** Four steps of setting up an 11-car connected vehicle network on a ring road. **b** Vehicles represented by *black circles* are placed on a single lane ring road. The *black arrow* represents the clockwise direction of the traffic flow. The *blue arrows* represent the flow of information in the network. **c** Transmitting vehicles (are highlighted as *green*). **d** Some of the transmitting vehicles become CCC vehicles (indicated by *black crosses*). **e** V2V links are setup between transmitting vehicles and CCC vehicles by assuming that each CCC vehicle can receive information from up to four connected vehicles ahead of it. (Color figure online)

motion information via V2V communication (transmitting vehicles) and we select a subset of these vehicles that can receive V2V information and may act on that using a CCC algorithm. Finally, we setup the V2V links based on proximity that represent the information flow between connected vehicles.

Here, we adopt the car-following model described in [3,8] to serve as a basis for developing a connected vehicle network with V2V communication. We consider identical vehicles traveling on a single lane so that the i-th vehicle follows the $i+1$-st vehicle; see Fig. 1a. The position of the i-th vehicle is denoted by s_i, its velocity is v_i, and ℓ represents the vehicle length. We place N cars on a circular road such that first vehicle follows the N-th vehicle, i.e., we have the periodic boundary conditions $s_{N+1} = s_1$, $v_{N+1} = v_1$. The total length of the road is $L + N\,\ell$, where L is called the effective road length.

A diagram of a conventional vehicle network is shown in Fig. 1b for $N = 11$ vehicles denoted by the black dots. The vehicles move along the ring in the counterclockwise direction where the blue arrows indicate the flow of information between vehicles. Consider that vehicle i uses the headway $h_i = s_{i+1} - s_i - \ell$ and the relative velocity $v_{i+1} - v_i$ to control its longitudinal motion using the car-following rule

$$\begin{aligned}\dot{s}_i &= v_i,\\ \dot{v}_i &= \alpha\left(V(s_{i+1}-s_i-\ell)-v_i\right)+\beta_1\,(v_{i+1}-v_i),\end{aligned} \tag{1}$$

where the gains $\alpha > 0$ and $\beta_1 \leq 0$ are associated with the headway and relative velocity, respectively.

The headway feedback term involves the nonlinear function $V(h)$ called the range policy or optimal velocity function. This satisfies the following properties:

1. $V(h)$ is continuous and monotonically increasing (the more sparse the traffic is, the faster the vehicles want to travel).
2. $V(h) \equiv 0$ for $h \leq h_{\rm st}$ (in dense traffic vehicles intend to stop).
3. $V(h) \equiv v_{\rm max}$ for $h \geq h_{\rm go}$ (in sparse traffic vehicles intend to travel with the maximum speed, also called free-flow speed).

These properties are satisfied by the function

$$V(h) = \begin{cases} 0, & \text{if} \quad h \leq h_{\rm st}\,,\\ \dfrac{v_{\rm max}}{2}\left[1-\cos\left(\pi\,\frac{h-h_{\rm st}}{h_{\rm go}-h_{\rm st}}\right)\right], & \text{if} \quad h_{\rm st} < h < h_{\rm go}\,,\\ v_{\rm max}, & \text{if} \quad h \geq h_{\rm go}, \end{cases} \tag{2}$$

that we will use in the rest of the paper. We remark that the analytical calculations presented in this paper do not require a specific range policy. Any function satisfying the properties 1–3 would result in similar qualitative results.

Now we select a few vehicles that are able to transmit information about their state using wireless V2V communication. For example, in Fig. 1c we select vehicles $i = 1, 3, 6, 7, 9, 11$ to be transmitting vehicles. Some of the transmitting vehicles in the network possess a CCC controller that can actuate the vehicle based on the information received from other vehicles. For example, in Fig. 1d we select vehicles $i = 1, 7$ to be CCC vehicles. Finally, to form a connected vehicle network, the CCC vehicles use information from transmitting vehicles downstream to control their longitudinal motion. If the i-th vehicle is a CCC vehicle then its control law becomes

$$\begin{aligned}\dot{s}_i &= v_i\,,\\ \dot{v}_i &= \alpha\left(V(s_{i+1}-s_i-\ell)-v_i\right)+\beta_1\,(v_{i+1}-v_i)\\ &\quad+\sum_{\sigma=2}^{\sigma_{\rm max}}\beta_{i\sigma}\,(v_{i+\sigma}-v_i)\,,\end{aligned} \tag{3}$$

where the last term represents a relative velocity feedback from vehicles, $i+\sigma$, where $\sigma = 2, \ldots, \sigma_{\rm max}$ that are beyond the line of sight. The corresponding gains are denoted by $\beta_{i\sigma} \geq 0$. When $i+\sigma > N$ we use $s_{i+\sigma} = s_{i+\sigma-N}$ and $v_{i+\sigma} = v_{i+\sigma-N}$. In Fig. 1e we see two links with link length $\sigma = 2$ and one link with link length $\sigma = 4$. In connected vehicle networks links up to $\sigma \approx 4$ were shown to have a significant benefit [9], so in the examples shown in this paper we consider $\sigma_{\rm max} = 4$, but the developed framework can be used for links of arbitrary length.

One can show that (3) admits a pseudo-equilibrium

$$s_i^* = v_i^*\,t + s_i^0, \quad i = 1, \ldots, N, \tag{4}$$

where all cars are equidistant and travel with the same velocity, that is,

$$\begin{aligned} s_{i+1}^0 - s_i^0 - \ell &= \frac{L}{N} = h^*, \quad i = 1, \ldots, N-1,\\ s_1^0 - s_N^0 - \ell &= \frac{L}{N} = h^*,\\ v_i^* &= v^* = V(h^*), \quad i = 1, \ldots, N\,. \end{aligned} \tag{5}$$

We define the perturbations

$$\widetilde{s}_i = s_i - s_i^*, \quad \widetilde{v}_i = v_i - v^*, \tag{6}$$

and approximate the network about the pseudo-equilibrium (4, 5) using first-order Taylor expansion:

$$\begin{aligned}\dot{\widetilde{s}}_i &= \widetilde{v}_i\,,\\ \dot{\widetilde{v}}_i &= p\,(\widetilde{s}_{i+1}-\widetilde{s}_i)+\beta_1\,(\widetilde{v}_{i+1}-\widetilde{v}_i)-\alpha\,\widetilde{v}_i\\ &\quad+\sum_{\sigma=2}^{\sigma_{\rm max}}\beta_{i\sigma}\,(\widetilde{v}_{i+\sigma}-\widetilde{v}_i),\end{aligned} \tag{7}$$

where

$$p = \alpha\,V'(h^*)\,, \tag{8}$$

and the prime denotes the derivative with respect to the headway h.

System (1) consists of $2N$ equations, and the same holds for system (7). When $\beta_{i\sigma} = 0$ for all $i = 1, \ldots, N$ and $\sigma = 2, \ldots, \sigma_{\max}$ we can simplify the stability analysis of the system by exploiting the cyclic symmetry of the system using modal analysis. In the next section we will establish our modal analysis for a general mistuned symmetric system.

3 Network-based analysis of cyclic systems with acyclic perturbations

In this section we develop methods for the linear modal analysis of systems with an underlying cyclic structure that is perturbed by long-range connections (that make the system acyclic). We write the Jacobian of the overall system as a sum of a block-circulant matrix (representing the unperturbed cyclic system) and perturbation (matrices representing the long-range connections). First we obtain the modes using a linear transformation for the unperturbed cyclic system. This is a well-known problem and was extensively discussed in [18]. We then develop a perturbation method to approximate the modes for the perturbed acyclic system around the cyclically symmetric configuration. We exploit the cyclic structure of the unperturbed system to reduce the complexity of calculations when solving for the modes of the perturbed acyclic system. As mentioned above, such a modal decomposition can be performed for systems with arbitrary numbers of nodes and an arbitrary number of perturbations without significant increase in complexity. Our network-based modal analysis also reveals how different parameters influence modal and system stability.

Assuming the state of the i-th node is described by the vector $\mathbf{x}_i = [x_i^{(1)}, \ldots, x_i^{(M)}]^{\mathrm{T}}$, its dynamics can be written as

$$\dot{\mathbf{x}}_i = \mathbf{g}(\mathbf{x}_i, \mathbf{x}_{i+1}, \cdots, \mathbf{x}_{i+N-1}) + \sum_{\sigma=0}^{\sigma_{\max}} \mathbf{h}_{i\sigma}(\mathbf{x}_i, \mathbf{x}_{i+\sigma})\varepsilon_{i\sigma}, \tag{9}$$

where $\mathbf{x}_{N+i} \equiv \mathbf{x}_i$ and $\mathbf{g} = [g^{(1)}, \ldots, g^{(M)}]^{\mathrm{T}}$ is a vector valued function that represents the cyclic coupling of the nodes. The vector valued functions $\mathbf{h}_{i\sigma} = [h_{i\sigma}^{(1)}, \ldots, h_{i\sigma}^{(M)}]^{\mathrm{T}}$ represent the acyclic perturbations to the cyclic structure, while $\varepsilon_{i\sigma}$ represents the magnitude of the perturbations. We assume that the system possesses a equilibrium where all the nodes are synchronized

$$\mathbf{x}_i \equiv \mathbf{x}^*, \tag{10}$$

for $i = 1, \ldots, N$ satisfying $\mathbf{g}(\mathbf{x}^*, \ldots, \mathbf{x}^*) = \mathbf{0}$ and $\mathbf{h}_{i\sigma}(\mathbf{x}^*, \mathbf{x}^*) = \mathbf{0}$.

By defining the perturbation

$$\mathbf{y}_i = \mathbf{x}_i - \mathbf{x}^*, \tag{11}$$

where $\mathbf{y}_i = [y_i^{(1)} \ldots y_i^{(N)}]^{\mathrm{T}}$, we linearize (9) around the synchronous equilibrium (10) and obtain

$$\dot{\mathbf{y}}_i = \sum_{j=1}^{N} \mathbf{C}_j \mathbf{y}_{i+j-1} + \sum_{\sigma=0}^{\sigma_{\max}} (\partial_1 \mathbf{h}_{i\sigma} \mathbf{y}_i + \partial_2 \mathbf{h}_{i\sigma} \mathbf{y}_{i+\sigma})\varepsilon_{i\sigma}, \tag{12}$$

where the $M \times M$ matrices $\mathbf{C}_j$, $\partial_1 \mathbf{h}_{i\sigma}$, $\partial_2 \mathbf{h}_{i\sigma}$ are given by

$$[\mathbf{C}_j]_{bd} = \left.\frac{\partial g^{(b)}}{\partial x_{i+j-1}^{(d)}}\right|_*, \quad [\partial_1 \mathbf{h}_{i\sigma}]_{bd} = \left.\frac{\partial h_{i\sigma}^{(b)}}{\partial x_i^{(d)}}\right|_*,$$
$$[\partial_2 \mathbf{h}_{i\sigma}]_{bd} = \left.\frac{\partial h_{i\sigma}^{(b)}}{\partial x_{i+\sigma}^{(d)}}\right|_*, \tag{13}$$

where the asterisk denotes that the derivatives are evaluated at the synchronous equilibrium. Notice that $\mathbf{C}_j$ does not depend on i because the nodes are cyclically coupled. By defining the state vector $\hat{\mathbf{y}} = [\mathbf{y}_1^{\mathrm{T}} \ldots \mathbf{y}_N^{\mathrm{T}}]^{\mathrm{T}}$ we can rewrite (12) into the compact form

$$\dot{\hat{\mathbf{y}}} = \hat{\mathbf{J}}\,\hat{\mathbf{y}}, \tag{14}$$

where the Jacobian

$$\hat{\mathbf{J}} = \hat{\mathbf{J}}_0 + \sum_{i_1=1}^{N} \sum_{\sigma_1=0}^{\sigma_{\max}} \hat{\mathbf{P}}(i_1, \sigma_1)\varepsilon_{i_1\sigma_1}, \tag{15}$$

is divided into parts corresponding to the cyclic system and the perturbations. Indeed, the cyclic coupling between the nodes is represented by

$$\hat{\mathbf{J}}_0 = \mathrm{circ}(\mathbf{C}_1, \ldots, \mathbf{C}_N) = \begin{bmatrix} \mathbf{C}_1 & \mathbf{C}_2 & \cdots & \mathbf{C}_N \\ \mathbf{C}_N & \mathbf{C}_1 & \cdots & \mathbf{C}_{N-1} \\ \vdots & \vdots & \ddots & \vdots \\ \mathbf{C}_2 & \mathbf{C}_3 & \cdots & \mathbf{C}_1 \end{bmatrix}, \tag{16}$$

that is a block-circulant matrix of type (M, N); see [18]. The terms

$$\hat{\mathbf{P}}(i_1,\sigma_1) = \mathbf{\Delta}_{i_1 i_1} \otimes \partial_1 \mathbf{h}_{i_1\sigma_1} + \mathbf{\Delta}_{i_1 i_1+\sigma_1} \otimes \partial_2 \mathbf{h}_{i_1\sigma_1}, \tag{17}$$

represent the perturbations to the cyclic structure where $\mathbf{\Delta}_{ij} \in \mathbb{R}^{N\times N}$ contains a "1" in the i-th row and the j-th column, and zeros everywhere else. The symbol $\otimes$ denotes the Kronecker product. Indeed, the matrix $\hat{\mathbf{P}}(i_1,\sigma_1)$ corresponds to a particular link of length σ_1 starting at node $i_1+\sigma_1$ and ending at node i_1, cf. Fig. 1e. In $\hat{\mathbf{P}}(i_1,\sigma_1)$ we use brackets instead of subscripts in order to improve the readability.

3.1 Modal analysis of cyclic systems

Before obtaining approximations of the modes for the system with acyclic perturbations we obtain the modes of the cyclic system; see [18]. In particular, we use a linear modal transformation that exploits the circulant structure of the Jacobian $\hat{\mathbf{J}}_0$ given in (15). When considering (14,15) with $\varepsilon_{i_1\sigma_1} = 0$, (16) can be represented as a linear combination of its generating elements using the Kronecker product

$$\hat{\mathbf{J}}_0 = \sum_{j=1}^{N} (\mathbf{A}_N)^{(j-1)} \otimes \mathbf{C}_j, \tag{18}$$

where the N-dimensional forward shift matrix $\mathbf{A}_N = [\,a_{ij}\,]$ contains elements defined as

$$a_{ij} = \begin{cases} 1 & \text{if} \quad j = i+1\,, \\ 0 & \text{otherwise}\,. \end{cases} \tag{19}$$

We define the linear coordinate transformation

$$\hat{\mathbf{y}} = \hat{\mathbf{T}}_0\,\hat{\mathbf{z}}\,, \tag{20}$$

with modal coordinates $\mathbf{z}_k = [z_k^{(1)} \ \dots \ z_k^{(M)}]^{\mathrm{T}}$, $\hat{\mathbf{z}} = [\mathbf{z}_1^{\mathrm{T}} \ \dots \ \mathbf{z}_N^{\mathrm{T}}]^{\mathrm{T}}$, and matrix

$$\hat{\mathbf{T}}_0 = \mathbf{T}_N \otimes \mathbf{I}_M. \tag{21}$$

Here $\mathbf{T}_N = \begin{bmatrix}\mathbf{e}_1 \cdots \mathbf{e}_N\end{bmatrix}$ and $\mathbf{e}_k$ is the k-th eigenvector of the forward shift matrix $\mathbf{A}_N$ corresponding to the k-th modal eigenvalue $\mathrm{e}^{i\frac{2\pi\,(k-1)}{N}}$, where $i^2 = -1$, $k = 1, \dots, N$, and $\mathbf{I}_M$ is the M-dimensional identity matrix. This transformation is also known as the discrete Fourier transformation; see [18].

Notice that the mode number $k = 1$ corresponds to a translational symmetry of the system, the mode numbers $k = 2, \dots, \lfloor \frac{N}{2} + 1 \rfloor$ correspond to having $k-1$ waves along the ring, while the mode numbers $k = \lceil \frac{N}{2} + 1 \rceil, \dots, N$ correspond to having $N-k+2$ waves along the ring; see [8,18]. Applying the modal transformation (20) the equation $\dot{\hat{\mathbf{y}}} = \hat{\mathbf{J}}_0\hat{\mathbf{y}}$ (cf. (14,15)) without perturbations can be rewritten as

$$\dot{\hat{\mathbf{z}}} = \hat{\mathbf{D}}_0\,\hat{\mathbf{z}}\,, \tag{22}$$

where the block-diagonal matrix $\hat{\mathbf{D}}_0 \in \mathbb{C}^{NM\times NM}$ is given by

$$\hat{\mathbf{D}}_0 = \hat{\mathbf{T}}_0^{-1}\hat{\mathbf{J}}_0\hat{\mathbf{T}}_0 = \mathrm{diag}([\hat{\mathbf{D}}_0]_k^k)\,. \tag{23}$$

In particular, the block

$$[\hat{\mathbf{D}}_0]_k^k = \sum_{j=1}^{N} \mathbf{C}_j \mathrm{e}^{i\frac{2\pi}{N}(k-1)(j-1)} \tag{24}$$

gives the dynamics of the k-th mode of the cyclic system. We note that the mode/block-eigenvector relationships for mode k can be formulated as

$$(\hat{\mathbf{J}}_0 - \mathbf{I}_N \otimes [\hat{\mathbf{D}}_0]_k^k)[\hat{\mathbf{T}}_0]_k = 0\,, \tag{25}$$

and

$$[\hat{\mathbf{T}}_0^{-1}]^k(\hat{\mathbf{J}}_0 - \mathbf{I}_N \otimes [\hat{\mathbf{D}}_0]_k^k) = 0\,, \tag{26}$$

where $[\hat{\mathbf{T}}_0]_k$ is the so-called k-th "block eigenvector," that is the k-th set of M columns of $\hat{\mathbf{T}}_0$ and $[\hat{\mathbf{T}}_0^{-1}]^k$ is the so-called k-th "left block eigenvector," that is the k-th set of M rows of $\hat{\mathbf{T}}_0^{-1}$. Formulae (25) and (26) will be used extensively to obtain approximations of modes and block eigenvectors for the perturbed system in the next subsection.

Note that the linear coordinate transformation simplifies the linear analysis of the system: the linear part is decoupled into N sets of complex differential equations representing the oscillation modes. Thus, the linear stability can be analyzed separately for each mode and the stability of the synchronous state (10) is ensured when all modes are stable.

3.2 Modal analysis of cyclic systems with acyclic perturbations

In this section we build upon the analysis of the cyclic system to obtain an approximation for the modes of the mistuned cyclic system (14,15) when $\varepsilon_{i_1\sigma_1} > 0$ are small for all $i_1 = 1, \ldots, N$, $\sigma_1 = 0, \ldots, \sigma_{\max}$.

We assume that $\hat{\mathbf{J}}$ can be transformed to a block-diagonal matrix $\hat{\mathbf{D}}$ using the transformation

$$\hat{\mathbf{z}} = \hat{\mathbf{T}}\,\hat{\mathbf{y}}, \tag{27}$$

yielding

$$\dot{\hat{\mathbf{z}}} = \hat{\mathbf{D}}\,\mathbf{z}\,, \tag{28}$$

with

$$\hat{\mathbf{D}} = \hat{\mathbf{T}}^{-1}\,\hat{\mathbf{J}}\,\hat{\mathbf{T}} = \mathrm{diag}([\hat{\mathbf{D}}]_k^k). \tag{29}$$

Indeed $[\hat{\mathbf{D}}]_k^k$ (k-th modal block) and $\big[\hat{\mathbf{T}}\big]_k$ (the k-th block eigenvector) satisfy the equation

$$(\hat{\mathbf{J}} - \mathbf{I}_N \otimes [\hat{\mathbf{D}}]_k^k)\big[\hat{\mathbf{T}}\big]_k = 0\,, \tag{30}$$

cf. (25).

We construct $\hat{\mathbf{D}}$ as an expansion about $\hat{\mathbf{D}}_0$ up to third-order in $\varepsilon_{i\,\sigma}$:

$$\begin{aligned}\hat{\mathbf{D}} = \hat{\mathbf{D}}_0 &+ \sum_{i_1=1}^{N}\sum_{\sigma_1=0}^{\sigma_{\max}} \hat{\mathbf{D}}^{(1)}\,\varepsilon_{i_1\sigma_1} \\ &+ \frac{1}{2}\sum_{i_1,i_2=1}^{N}\sum_{\sigma_1,\sigma_2=0}^{\sigma_{\max}} \hat{\mathbf{D}}^{(1,2)}\,\varepsilon_{i_1\sigma_1}\varepsilon_{i_2\sigma_2} \\ &+ \frac{1}{6}\sum_{i_1,i_2,i_3=1}^{N}\sum_{\sigma_1,\sigma_2,\sigma_3=0}^{\sigma_{\max}} \hat{\mathbf{D}}^{(1,2,3)}\,\varepsilon_{i_1\sigma_1}\varepsilon_{i_2\sigma_2}\varepsilon_{i_3\sigma_3} \\ &+ \cdots\,,\end{aligned} \tag{31}$$

where we introduced the compact notation

$$\begin{aligned}\mathbf{M}^{(1)} &= \mathbf{M}_1(i_1,\sigma_1),\\ \mathbf{M}^{(1,2)} &= \mathbf{M}_2(i_1,\sigma_1,i_2,\sigma_2),\\ \mathbf{M}^{(1,2,3)} &= \mathbf{M}_3(i_1,\sigma_1,i_2,\sigma_2,i_3,\sigma_3).\end{aligned} \tag{32}$$

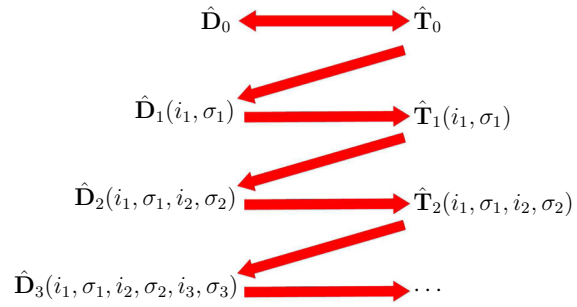

Fig. 2 Diagram showing the sequential method of obtaining the approximations for the modal blocks and block eigenvectors of the perturbed system by solving (30) and (29)

In order to be able to derive the coefficient matrices in (31) we expand $\hat{\mathbf{T}}$ up to second-order

$$\begin{aligned}\hat{\mathbf{T}} = \hat{\mathbf{T}}_0 &+ \sum_{i_1=1}^{N}\sum_{\sigma_1=0}^{\sigma_{\max}} \hat{\mathbf{T}}^{(1)}\,\varepsilon_{i_1\sigma_1} \\ &+ \frac{1}{2}\sum_{i_1,i_2=1}^{N}\sum_{\sigma_1,\sigma_2=0}^{\sigma_{\max}} \hat{\mathbf{T}}^{(1,2)}\,\varepsilon_{i_1\sigma_1}\varepsilon_{i_2\sigma_2} + \cdots\,.\end{aligned} \tag{33}$$

Since we already know $\hat{\mathbf{D}}_0$ and $\hat{\mathbf{T}}_0$ from (23,24) and (21), respectively, we use (30) and (29) sequentially to obtain the higher-order terms of $\hat{\mathbf{D}}$ and $\hat{\mathbf{T}}$ as depicted in Fig. 2.

In particular, to determine the higher-order terms in $[\hat{\mathbf{D}}]_k^k$ we differentiate (30) with respect to $\varepsilon_{i\,\sigma}$, while to obtain the higher-order terms of $[\hat{\mathbf{T}}]_k$ we compare the left and right hand sides of (29). To obtain the first-order perturbation of the dynamics of the k-th mode $[\hat{\mathbf{D}}^{(1)}]_k^k$ for an arbitrary i_1, σ_1 we take the derivative of (30) with respect to $\varepsilon_{i_1\sigma_1}$ pair (denoted by ∂_{ε_1}) to obtain

$$\begin{aligned}&\Big(\partial_{\varepsilon_1}\hat{\mathbf{J}} - \mathbf{I}_N \otimes \partial_{\varepsilon_1}[\hat{\mathbf{D}}]_k^k\Big)[\hat{\mathbf{T}}]_k \\ &+ \Big(\hat{\mathbf{J}} - \mathbf{I}_N \otimes [\hat{\mathbf{D}}]_k^k\Big)\partial_{\varepsilon_1}[\hat{\mathbf{T}}]_k = 0.\end{aligned} \tag{34}$$

We then evaluate this at $\varepsilon_{i_1\sigma_1} = 0$, yielding

$$\begin{aligned}&\big(\hat{\mathbf{P}}^{(1)} - \mathbf{I}_N \otimes [\hat{\mathbf{D}}^{(1)}]_k^k\big)[\hat{\mathbf{T}}_0]_k \\ &+ \big(\hat{\mathbf{J}}_0 - \mathbf{I}_N \otimes [\hat{\mathbf{D}}_0]_k^k\big)[\hat{\mathbf{T}}^{(1)}]_k = 0,\end{aligned} \tag{35}$$

where we use the compact notation $\mathbf{M}^{(1)} = \mathbf{M}(i_1,\sigma_1)$; cf. (32) and see (15,16,17). Multiplying (35) with $[\hat{\mathbf{T}}_0^{-1}]^k$ from the left and using (26) we can eliminate the second term, that is,

$$[\hat{\mathbf{T}}_0^{-1}]^k\big(\hat{\mathbf{P}}^{(1)} - \mathbf{I}_N \otimes [\hat{\mathbf{D}}^{(1)}]_k^k\big)[\hat{\mathbf{T}}_0]_k = 0, \tag{36}$$

which can be simplified and solved for

$$[\hat{\mathbf{D}}^{(1)}]_k^k = [\hat{\mathbf{T}}_0^{-1}]^k \, \hat{\mathbf{P}}^{(1)} [\hat{\mathbf{T}}_0]_k, \tag{37}$$

We can substitute the definition (17) of $\hat{\mathbf{P}}^{(1)}$ to obtain a general expression for the first-order perturbation of the k mode due to a link between nodes i_1 and $i_1+\sigma_1$:

$$\begin{aligned}[\hat{\mathbf{D}}^{(1)}]_k^k &= [\hat{\mathbf{D}}_1(i_1,\sigma_1)]_k^k \\ &= \frac{1}{N}\Big(\partial_1 \mathbf{h}_{i_1\sigma_1} + \mathrm{e}^{i\frac{2\pi}{N}\sigma_1(k-1)}\partial_2 \mathbf{h}_{i_1\sigma_1}\Big).\end{aligned} \tag{38}$$

To expand the modal dynamics up to second-order in terms of mistunings we must first obtain the expansion of matrix $\hat{\mathbf{T}}$ and its block eigenvectors up to first-order. Notice that the expansion for $\hat{\mathbf{T}}^{-1}$ can be written as

$$\begin{aligned}\hat{\mathbf{T}}^{-1} \approx \hat{\mathbf{T}}_0^{-1} &- \sum_{i_1=1}^{N}\sum_{\sigma_1=0}^{\sigma_{\max}} \hat{\mathbf{T}}_0^{-1}\hat{\mathbf{T}}^{(1)}\hat{\mathbf{T}}_0^{-1}\varepsilon_{i_1\sigma_1} \\ &+ \sum_{i_1,i_2=1}^{N}\sum_{\sigma_1,\sigma_2=0}^{\sigma_{\max}} \Big(\hat{\mathbf{T}}_0^{-1}\hat{\mathbf{T}}^{(1)}\hat{\mathbf{T}}_0^{-1}\hat{\mathbf{T}}^{(2)}\hat{\mathbf{T}}_0^{-1} \\ &- \frac{1}{2}\hat{\mathbf{T}}_0^{-1}\hat{\mathbf{T}}^{(1,2)}\hat{\mathbf{T}}_0^{-1}\Big)\varepsilon_{i_1\sigma_1}\varepsilon_{i_2\sigma_2} + \cdots,\end{aligned} \tag{39}$$

where we exploited the Neumann series, given by

$$(\mathbf{I}+\mathbf{M})^{-1} \approx \mathbf{I} - \mathbf{M} + \mathbf{M}^2 + \cdots, \tag{40}$$

where $\mathbf{M}$ is a square matrix whose eigenvalues are less than 1 and $\mathbf{I}$ is an identity matrix. Substituting (31), (33) and (39) into (29) and matching the first-order terms in $\varepsilon_{i_1\sigma_1}$ yields

$$\begin{aligned}\sum_{i_1=1}^{N}\sum_{\sigma_1=0}^{\sigma_{\max}} \hat{\mathbf{D}}^{(1)}\varepsilon_{i_1\sigma_1} = \sum_{i_1=1}^{N}\sum_{\sigma_1=0}^{\sigma_{\max}} \Big(&- \hat{\mathbf{T}}_0^{-1}\hat{\mathbf{T}}^{(1)}\hat{\mathbf{T}}_0^{-1}\hat{\mathbf{J}}_0\hat{\mathbf{T}}_0 \\ &+ \hat{\mathbf{T}}_0^{-1}\hat{\mathbf{P}}^{(1)}\hat{\mathbf{T}}_0 + \hat{\mathbf{T}}_0^{-1}\hat{\mathbf{J}}_0\hat{\mathbf{T}}^{(1)}\Big)\varepsilon_{i_1\sigma_1}.\end{aligned} \tag{41}$$

We equate the terms corresponding to a perturbation corresponding to an arbitrary i_1, σ_1 pair and use (23) to simplify the formula to obtain a Sylvester equation

$$\hat{\mathbf{D}}_0\hat{\mathbf{U}}^{(1)} - \hat{\mathbf{U}}^{(1)}\hat{\mathbf{D}}_0 = \hat{\mathbf{D}}^{(1)} - \hat{\mathbf{T}}_0^{-1}\hat{\mathbf{P}}^{(1)}\hat{\mathbf{T}}_0, \tag{42}$$

for the matrix $\hat{\mathbf{U}}^{(1)} = \hat{\mathbf{T}}_0^{-1}\hat{\mathbf{T}}^{(1)}$ of $(MN)^2$ unknowns.

The complexity of (42) can be reduced significantly by exploiting the cyclic structure of the unperturbed system. In (42), $\hat{\mathbf{U}}^{(1)}$ is multiplied by block-diagonal matrices from the left and right. Thus, the coefficients contained by $[\hat{\mathbf{U}}^{(1)}]_\ell^k$ remain in the k-th block row and ℓ-th block column after the multiplications, which yields

$$\begin{aligned}&[\hat{\mathbf{D}}_0]_k^k[\hat{\mathbf{U}}^{(1)}]_\ell^k - [\hat{\mathbf{U}}^{(1)}]_\ell^k[\hat{\mathbf{D}}_0]_\ell^\ell \\ &= [\hat{\mathbf{D}}^{(1)}]_\ell^k - [\hat{\mathbf{T}}_0^{-1}]^k \, \hat{\mathbf{P}}^{(1)}[\hat{\mathbf{T}}_0]_\ell.\end{aligned} \tag{43}$$

Using (17) and (38), this can be written as

$$\begin{aligned}&[\hat{\mathbf{D}}_0]_k^k[\hat{\mathbf{U}}^{(1)}]_\ell^k - [\hat{\mathbf{U}}^{(1)}]_\ell^k[\hat{\mathbf{D}}_0]_\ell^\ell \\ &= \frac{1}{N}\mathrm{e}^{i\frac{2\pi}{N}(i_1-1)(\ell-k)}\Big(\partial_1 \mathbf{h}_{i_1\sigma_1} + \mathrm{e}^{i\frac{2\pi}{N}\sigma_1(\ell-1)}\partial_2 \mathbf{h}_{i_1\sigma_1}\Big) \\ &\quad (\delta_{k\ell}-1),\end{aligned} \tag{44}$$

where $\delta_{k\ell}$ denotes the Kronecker delta. This Sylvester equation can be rewritten into the standard form of a linear algebraic equation

$$\mathbf{A}_{k\,\ell}^{(1)}\mathbf{b}_{k\,\ell}^{(1)} = \mathbf{c}_{k\,\ell}^{(1)}, \tag{45}$$

where

$$\mathbf{A}_{k\,\ell}^{(1)} = \mathbf{I}_M \otimes [\hat{\mathbf{D}}_0]_k^k - [\hat{\mathbf{D}}_0^{\mathrm{T}}]_\ell^\ell \otimes \mathbf{I}_M, \tag{46}$$

and

$$\mathbf{b}_{k\,\ell}^{(1)} = \mathrm{vec}([\hat{\mathbf{U}}^{(1)}]_\ell^k). \tag{47}$$

Here $\mathrm{vec}(\cdot)$ is the vectorization operator that stacks the columns of a matrix into a column vector. Similarly, $\mathbf{c}_{k\,\ell}^{(1)}$ is the vectorization of the right hand side of (44). Thus, by exploiting the cyclic structure of the unperturbed system (18) we need to solve N^2 decoupled linear equations each with M^2 unknowns. In contrast (42) would require us to solve $(MN)^2$ coupled equations. For the diagonal $M \times M$ blocks of $\hat{\mathbf{U}}^{(1)}$, equation (45) has multiple possible solutions due to a nonzero nullity. Here we set

$$[\hat{\mathbf{U}}^{(1)}]_k^k = \mathbf{0}. \tag{48}$$

Once all the $M \times M$ blocks of $\hat{\mathbf{U}}^{(1)}$ are solved for, we can calculate $\hat{\mathbf{T}}^{(1)} = \hat{\mathbf{T}}_0\hat{\mathbf{U}}^{(1)}$.

To obtain the second-order perturbation of the dynamics of the k-th mode $[\hat{\mathbf{D}}^{(1,2)}]_k^k$ for an arbitrary $i_1, \sigma_1, i_2, \sigma_2$ quadruple we take the derivative of (34) with respect to $\varepsilon_{i_2\sigma_2}$ (denoted by ∂_{ε_2}) yielding

$$\begin{aligned}&\Big(\partial_{\varepsilon_1}\partial_{\varepsilon_2}\hat{\mathbf{J}} - \mathbf{I}_N\otimes\partial_{\varepsilon_1}\partial_{\varepsilon_2}[\hat{\mathbf{D}}]_k^k\Big)[\hat{\mathbf{T}}]_k\\&\quad+\Big(\partial_{\varepsilon_1}\hat{\mathbf{J}} - \mathbf{I}_N\otimes\partial_{\varepsilon_1}[\hat{\mathbf{D}}]_k^k\Big)\partial_{\varepsilon_2}[\hat{\mathbf{T}}]_k\\&\quad+\Big(\partial_{\varepsilon_2}\hat{\mathbf{J}} - \mathbf{I}_N\otimes\partial_{\varepsilon_2}[\hat{\mathbf{D}}]_k^k\Big)\partial_{\varepsilon_1}[\hat{\mathbf{T}}]_k\\&\quad+\Big(\hat{\mathbf{J}} - \mathbf{I}_N\otimes[\hat{\mathbf{D}}]_k^k\Big)\partial_{\varepsilon_1}\partial_{\varepsilon_2}[\hat{\mathbf{T}}]_k = 0,\end{aligned}\tag{49}$$

and evaluate this at $\varepsilon_{i_1\sigma_1}=0$, $\varepsilon_{i_2\sigma_2}=0$ to get

$$\begin{aligned}&\frac{1}{2}\mathbf{I}_N\otimes([\hat{\mathbf{D}}^{(1,2)}]_k^k+[\hat{\mathbf{D}}^{(2,1)}]_k^k)[\hat{\mathbf{T}}_0]_k\\&\quad=\big(\hat{\mathbf{P}}^{(1)}-\mathbf{I}_N\otimes[\hat{\mathbf{D}}^{(1)}]_k^k\big)[\hat{\mathbf{T}}^{(2)}]_k\\&\qquad+\big(\hat{\mathbf{P}}^{(2)}-\mathbf{I}_N\otimes[\hat{\mathbf{D}}^{(2)}]_k^k\big)[\hat{\mathbf{T}}^{(1)}]_k\\&\qquad+\frac{1}{2}\big(\hat{\mathbf{J}}_0-\mathbf{I}_N\otimes[\hat{\mathbf{D}}_0]_k^k\big)\big([\hat{\mathbf{T}}^{(1,2)}]_k+[\hat{\mathbf{T}}^{(2,1)}]_k\big),\end{aligned}\tag{50}$$

where we used the compact notation $\mathbf{M}^{(1,2)} = \mathbf{M}_2(i_1,\sigma_1,i_2,\sigma_2)$, cf. (32) and see (15,16,17). We eliminate the last term in the expression above by multiplying by $[\hat{\mathbf{T}}_0^{-1}]^k$ from the left and use (26) to obtain

$$\begin{aligned}&[\hat{\mathbf{D}}^{(1,2)}]_k^k+[\hat{\mathbf{D}}^{(2,1)}]_k^k\\&\quad=2[\hat{\mathbf{T}}_0^{-1}]^k\big(\hat{\mathbf{P}}^{(1)}-\mathbf{I}_N\otimes[\hat{\mathbf{D}}^{(1)}]_k^k\big)[\hat{\mathbf{T}}^{(2)}]_k\\&\qquad+2[\hat{\mathbf{T}}_0^{-1}]^k\big(\hat{\mathbf{P}}^{(2)}-\mathbf{I}_N\otimes[\hat{\mathbf{D}}^{(2)}]_k^k\big)[\hat{\mathbf{T}}^{(1)}]_k.\end{aligned}\tag{51}$$

Since the above expression contains two unknowns $([\hat{\mathbf{D}}^{(1,2)}]_k^k$ and $[\hat{\mathbf{D}}^{(2,1)}]_k^k)$ for each $i_1,\sigma_1,i_2,\sigma_2$ quadruple, we have the freedom to set

$$[\hat{\mathbf{D}}^{(1,2)}]_k^k=2[\hat{\mathbf{T}}_0^{-1}]^k\big(\hat{\mathbf{P}}^{(1)}-\mathbf{I}_N\otimes[\hat{\mathbf{D}}^{(1)}]_k^k\big)[\hat{\mathbf{T}}^{(2)}]_k.\tag{52}$$

Since $[\hat{\mathbf{T}}_0^{-1}]^k(\mathbf{I}_N\otimes[\hat{\mathbf{D}}^{(1)}]_k^k)[\hat{\mathbf{T}}^{(2)}]_k=0$ we obtain the simplified form

$$[\hat{\mathbf{D}}^{(1,2)}]_k^k=2[\hat{\mathbf{T}}_0^{-1}]^k\hat{\mathbf{P}}^{(1)}[\hat{\mathbf{T}}^{(2)}]_k.\tag{53}$$

Using (17) this can be written as

$$\begin{aligned}[\hat{\mathbf{D}}^{(1,2)}]_k^k&=[\hat{\mathbf{D}}_2(i_1,\sigma_1,i_2,\sigma_2)]_k^k\\&=\sum_{j=1}^{N}\frac{2}{N}\mathrm{e}^{i\frac{2\pi}{N}(i_1-1)(j-k)}\big(\partial_1\mathbf{h}_{i_1\sigma_1}\\&\qquad+\mathrm{e}^{i\frac{2\pi}{N}\sigma_1(j-1)}\partial_2\mathbf{h}_{i_1\sigma_1}\big)[\hat{\mathbf{U}}^{(2)}]_k^j,\end{aligned}\tag{54}$$

where the components of $\hat{\mathbf{U}}^{(2)} = \hat{\mathbf{U}}_1(i_2,\sigma_2) = \hat{\mathbf{T}}_0^{-1}\hat{\mathbf{T}}_1(i_2,\sigma_2)$ are given by the solution of (45).

To expand the modal dynamics up to third-order we must first obtain the expansion of matrix $\hat{\mathbf{T}}$ up to second-order. The process is similar to the process of expanding $\hat{\mathbf{T}}$ up to first-order; cf. (41–48). Substituting (31), (33) and (39) into (29) and collecting the second-order terms yields

$$\begin{aligned}&\frac{1}{2}\sum_{i_1,i_2=1}^{N}\sum_{\sigma_1,\sigma_2=0}^{\sigma_{\max}}\hat{\mathbf{D}}^{(1,2)}\varepsilon_{i_1\sigma_1}\varepsilon_{i_2\sigma_2}\\&\quad=\sum_{i_1,i_2=1}^{N}\sum_{\sigma_1,\sigma_2=0}^{\sigma_{\max}}\Big(-\frac{1}{2}\hat{\mathbf{T}}_0^{-1}\hat{\mathbf{T}}^{(1,2)}\hat{\mathbf{T}}_0^{-1}\hat{\mathbf{J}}_0\hat{\mathbf{T}}_0\\&\qquad+\hat{\mathbf{T}}_0^{-1}\hat{\mathbf{T}}^{(1)}\hat{\mathbf{T}}_0^{-1}\hat{\mathbf{T}}^{(2)}\hat{\mathbf{T}}_0^{-1}\hat{\mathbf{J}}_0\hat{\mathbf{T}}_0-\hat{\mathbf{T}}_0^{-1}\hat{\mathbf{T}}^{(1)}\hat{\mathbf{T}}_0^{-1}\hat{\mathbf{P}}^{(2)}\hat{\mathbf{T}}_0\\&\qquad-\hat{\mathbf{T}}_0^{-1}\hat{\mathbf{T}}^{(1)}\hat{\mathbf{T}}_0^{-1}\hat{\mathbf{J}}_0\hat{\mathbf{T}}^{(2)}+\hat{\mathbf{T}}_0^{-1}\hat{\mathbf{P}}^{(1)}\hat{\mathbf{T}}^{(2)}\\&\qquad+\frac{1}{2}\hat{\mathbf{T}}_0^{-1}\hat{\mathbf{J}}_0\hat{\mathbf{T}}^{(1,2)}\Big)\varepsilon_{i_1\sigma_1}\varepsilon_{i_2\sigma_2}.\end{aligned}\tag{55}$$

Equating the terms corresponding to $\varepsilon_{i_1\sigma_1}\varepsilon_{i_2\sigma_2}$, and using (23) and (42) and some algebraic manipulation we obtain the Sylvester equation

$$\begin{aligned}&\hat{\mathbf{D}}_0\hat{\mathbf{U}}^{(1,2)}-\hat{\mathbf{U}}^{(1,2)}\hat{\mathbf{D}}_0=\hat{\mathbf{D}}^{(1,2)}\\&\quad+2\hat{\mathbf{U}}^{(1)}\hat{\mathbf{D}}^{(2)}-2\hat{\mathbf{T}}_0^{-1}\hat{\mathbf{P}}^{(1)}\hat{\mathbf{T}}_0\hat{\mathbf{U}}^{(2)},\end{aligned}\tag{56}$$

for the matrix $\hat{\mathbf{U}}^{(1,2)}=\hat{\mathbf{T}}_0^{-1}\hat{\mathbf{T}}^{(1,2)}$.

We again compare individual blocks on the two sides of (56) and reduce it to a low-order Sylvester equation

$$\begin{aligned}&[\hat{\mathbf{D}}_0]_k^k[\hat{\mathbf{U}}^{(1,2)}]_\ell^k-[\hat{\mathbf{U}}^{(1,2)}]_\ell^k[\hat{\mathbf{D}}_0]_\ell^\ell\\&\quad=[\hat{\mathbf{D}}^{(1,2)}]_\ell^k+2[\hat{\mathbf{U}}^{(1)}]_\ell^k[\hat{\mathbf{D}}^{(2)}]_\ell^\ell\\&\qquad-2[\hat{\mathbf{T}}_0^{-1}]^k\hat{\mathbf{P}}^{(1)}\hat{\mathbf{T}}_0[\hat{\mathbf{U}}^{(2)}]_\ell.\end{aligned}\tag{57}$$

Using (38) this becomes

$$\begin{aligned}&[\hat{\mathbf{D}}_0]_k^k[\hat{\mathbf{U}}^{(1,2)}]_\ell^k-[\hat{\mathbf{U}}^{(1,2)}]_\ell^k[\hat{\mathbf{D}}_0]_\ell^\ell\\&\quad=\frac{2}{N}[\hat{\mathbf{U}}^{(1)}]_\ell^k(\partial_1\mathbf{h}_{i_2\sigma_2}+\mathbf{e}^{i\frac{2\pi}{N}\sigma_2(\ell-1)}\partial_2\mathbf{h}_{i_2\sigma_2})\\&\qquad-\sum_{j=1}^{N}\frac{2}{N}\mathrm{e}^{i\frac{2\pi}{N}(i_1-1)(j-k)}\Big(\partial_1\mathbf{h}_{i_1\sigma_1}\\&\qquad+\mathrm{e}^{i\frac{2\pi}{N}\sigma_1(j-1)}\partial_2\mathbf{h}_{i_1\sigma_1}\Big)[\hat{\mathbf{U}}^{(2)}]_\ell^j(1-\delta_{k\ell}).\end{aligned}\tag{58}$$

that can be written into the form of a linear algebraic equation

$$\mathbf{A}_{k\,\ell}^{(1,2)}\,\mathbf{b}_{k\,\ell}^{(1,2)}=\mathbf{c}_{k\,\ell}^{(1,2)},\tag{59}$$

where

$$\mathbf{A}^{(1,2)}_{k\,\ell} = \mathbf{I}_M \otimes [\hat{\mathbf{D}}_0]^k_k - [\hat{\mathbf{D}}_0^{\mathrm{T}}]^\ell_\ell \otimes \mathbf{I}_M, \tag{60}$$

and

$$\mathbf{b}^{(1,2)}_{k\,\ell} = \mathrm{vec}([\hat{\mathbf{U}}^{(1,2)}]^k_\ell), \tag{61}$$

and $\mathbf{c}^{(1,2)}_{k\ell}$ is the vectorization of the right hand side of (58); cf. (45, 46, 47). Here again we need to solve N^2 decoupled equations equations with M^2 unknowns. In contrast in (57) would require us to solve $(NM)^2$ coupled equations.

The third-order perturbation for the dynamics of the k-th mode can then be obtained similarly to the way the first- and second-order perturbations were obtained. The detailed derivation is given in "Appendix 1." The result can be simplified to

$$\begin{aligned}[\hat{\mathbf{D}}^{(1,2,3)}]^k_k &= [\hat{\mathbf{D}}_3(i_1,\sigma_1,i_2,\sigma_2,i_3,\sigma_3)]^k_k \\ &= \frac{3}{N}\sum_{j=1}^{N} \mathrm{e}^{i\frac{2\pi}{N}(i_1-1)(j-k)}(\partial_1\mathbf{h}_{i_1\sigma_1} \\ &\quad + \mathrm{e}^{i\frac{2\pi}{N}\sigma_1(j-1)}\partial_2\mathbf{h}_{i_1\sigma_1})[\hat{\mathbf{U}}^{(2,3)}]^j_k,\end{aligned} \tag{62}$$

where the compact notation $\mathbf{M}^{(1,2,3)} = \mathbf{M}(i_1,\sigma_1,i_2,\sigma_2,i_3,\sigma_3)$ was used [cf. (32)]. Using (18), (38), (54) and (62) the dynamics of the k-th mode can be expressed by

$$\dot{\mathbf{z}}_k = [\hat{\mathbf{D}}]^k_k \mathbf{z}_k, \tag{63}$$

where

$$\begin{aligned}[\hat{\mathbf{D}}]^k_k &= \sum_{j=1}^{N}\mathbf{C}_j\mathrm{e}^{i\frac{2\pi}{N}(k-1)(j-1)} + \frac{1}{N}\sum_{i_1=1}^{N}\sum_{\sigma_1=0}^{\sigma_{\max}}\Big(\partial_1\mathbf{h}_{i_1\sigma_1} \\ &\quad + \mathrm{e}^{i\frac{2\pi}{N}\sigma_1(k-1)}\partial_2\mathbf{h}_{i_1\sigma_1}\Big)\varepsilon_{i_1\sigma_1} \\ &\quad + \frac{1}{N}\sum_{i_1,i_2=1}^{N}\sum_{\sigma_1,\sigma_2=0}^{\sigma_{\max}}\sum_{j=1}^{N}\mathrm{e}^{i\frac{2\pi}{N}(i_1-1)(j-k)}\big(\partial_1\mathbf{h}_{i_1\sigma_1} \\ &\quad + \mathrm{e}^{i\frac{2\pi}{N}\sigma_1(j-1)}\partial_2\mathbf{h}_{i_1\sigma_1}\big)[\hat{\mathbf{U}}^{(2)}]^j_k\varepsilon_{i_1\sigma_1}\varepsilon_{i_2\sigma_2} \\ &\quad + \frac{1}{2N}\sum_{i_1,i_2,i_3=1}^{N}\sum_{\sigma_1,\sigma_2,\sigma_3=0}^{\sigma_{\max}}\sum_{j=1}^{N}\mathrm{e}^{i\frac{2\pi}{N}(i_1-1)(j-k)} \\ &\quad (\partial_1\mathbf{h}_{i_1\sigma_1} + \mathrm{e}^{i\frac{2\pi}{N}\sigma_1(j-1)}\partial_2\mathbf{h}_{i_1\sigma_1})[\hat{\mathbf{U}}^{(2,3)}]^j_k \\ &\quad \varepsilon_{i_1\sigma_1}\varepsilon_{i_2\sigma_2}\varepsilon_{i_3\sigma_3}\,,\end{aligned} \tag{64}$$

and $[\hat{\mathbf{U}}^{(2)}]$ and $[\hat{\mathbf{U}}^{(2,3)}]$ are the solutions of (42) and (56), respectively.

That is we obtained N decoupled systems of M linear complex ordinary differential equations. Each system can then be separately analyzed to estimate the stability of the corresponding mode (assuming that the perturbations are small). To evaluate the linear stability of the synchronous state (10) we calculate the characteristic polynomial for mode k, given by

$$\det(\lambda\mathbf{I}_M - [\hat{\mathbf{D}}]^k_k) = 0, \tag{65}$$

and solve for its M eigenvalues $\lambda \in \mathbb{C}$. Indeed, the synchronous solution is stable when all modes are stable.

4 Modal approximation for heterogeneous connected vehicle network

In this section we analyze the connected vehicle network (1) using the framework developed above. First, we decompose the underlying cyclic system with nearest neighbor coupling and analyze the linear stability of the corresponding modes. Then, we use the developed perturbation analysis to approximate the modes in the presence of long-range links. Decoupling the modes of the connected vehicle network allows us to analyze the linear stability of the modes individually and characterize the oscillations that arise when these modes lose their stability. This allows us to study the effects of long-range V2V links on the stability of connected vehicle networks

Using the vector notation $\mathbf{y}_i = \mathrm{col}\,[\widetilde{s}_i \;\; \widetilde{v}_i]$, we can rewrite the dynamics of the i-th car (7) around the uniform flow as

$$\dot{\mathbf{y}}_i = \mathbf{C}_0\mathbf{y}_i + \mathbf{C}_1\mathbf{y}_{i+1} + \sum_{\sigma=2}^{\sigma_{\max}}(\partial_1\mathbf{h}_{i\sigma}\mathbf{y}_i + \partial_2\mathbf{h}_{i\sigma}\mathbf{y}_{i+\sigma})\beta_{i\sigma}\,, \tag{66}$$

(cf. 12). Here

$$\mathbf{C}_0 = \begin{bmatrix} 0 & 1 \\ -p & -\alpha-\beta_1 \end{bmatrix}, \quad \mathbf{C}_1 = \begin{bmatrix} 0 & 0 \\ p & \beta_1 \end{bmatrix}, \tag{67}$$

represent the nearest neighbor coupling,

$$\partial_1\mathbf{h}_{i\sigma} = \begin{bmatrix} 0 & 0 \\ 0 & -1 \end{bmatrix}, \quad \partial_2\mathbf{h}_{i\sigma} = \begin{bmatrix} 0 & 0 \\ 0 & 1 \end{bmatrix}, \tag{68}$$

correspond to the long-range connections, cf. (13) and $\beta_{i\sigma}$ stands for $\varepsilon_{i\sigma}$. Then we write (66) into the form (14,15) where

$$\hat{\mathbf{J}}_0 = \text{circ}(\mathbf{C}_0, \mathbf{C}_1, \mathbf{0}, \ldots, \mathbf{0}) = (\mathbf{I}_N \otimes \mathbf{C}_0 + \mathbf{A}_N \otimes \mathbf{C}_1), \tag{69}$$

[cf. (16,18)] and $\hat{\mathbf{P}}(i_1, \sigma_1)$ is defined in (17).

4.1 Modal analysis of connected vehicle network with nearest neighbor coupling

Prior to performing the linear modal analysis on the heterogeneous connected vehicle network, we first find the modes for the homogenous network, i.e., (66) with $\beta_{i\,\sigma} = 0$. This analysis was performed in detail in [3] and here we summarize the main findings. Performing the coordinate transformation (20) we obtain the dynamics of the k-th mode to be

$$[\hat{\mathbf{D}}_0]_k^k = \begin{bmatrix} 0 & 1 \\ p\,\eta_{k1} & \beta_1\eta_{k1} - \alpha \end{bmatrix}, \tag{70}$$

[cf. (24)] where

$$\eta_{k\,\ell} = \mathrm{e}^{i\frac{2\pi}{N}(k-1)} - \mathrm{e}^{i\frac{2\pi}{N}(\ell-1)}, \tag{71}$$

for $k,\ \ell = 1,\ \ldots,\ N$. Note that the dynamics of modes k and $N-k+2$ are complex conjugates of each other. Mode $k = 1$ corresponds to a translational symmetry of the system, see [20]. This mode does not become unstable for $\alpha > 0$. We also remark that for even N, there is another special mode $k = N/2+1$ which does not have a complex conjugate mode. This mode remains stable for $\alpha + 2\beta_1 > 0$.

Modes k and $N-k+2$ lose stability at a critical value of $p = \alpha\, V'(h^*)$ given by

$$p_k = \tfrac{1}{2}(2\beta_1+\alpha)\Big((2\beta_1+\alpha)\tan^2\left(\tfrac{(k-1)\,\pi}{N}\right)+\alpha\Big), \tag{72}$$

and the stability of these modes is lost to oscillations of frequencies

$$\omega_k = (2\beta_1 + \alpha)\tan\left(\tfrac{(k-1)\,\pi}{N}\right), \tag{73}$$

for $k = 2,\ \ldots,\ N$. Since (72) is monotonically increasing with k when $2 \le k \le \lfloor \frac{N}{2}+1 \rfloor$, the modes lose stability in the increasing order of mode number k. Thus, the uniform flow loses stability when modes 2 (and N) lose stability for the cyclically symmetric system with nearest neighbor coupling. At the linear level, the oscillations can be characterized by the modal coordinates $\mathbf{z}_k$ and $\mathbf{z}_{N+2-k}$. In order to perform a similar analysis for a connected vehicle network that includes long-range V2V links, we perform perturbation analysis to decouple the modes.

4.2 Stability analysis of connected vehicle network with long-range V2V connections

Now we consider the case that $\beta_{i_1\sigma_1}$ are small for all $i_1 = 1, \ldots, N$ and $\sigma_1 = 2, \ldots, \sigma_{\max}$. Considering (66) and using (30) with the approximations defined in (31), (33) and (39) we can obtain the perturbations to the modal dynamics and the modal transformation. We use (38) to obtain the first-order perturbation for the dynamics of the k-th mode associated with a link of length σ_1 terminated at vehicle i_1. This reads

$$[\hat{\mathbf{D}}_1(i_1, \sigma_1)]_k^k = \begin{bmatrix} 0 & 0 \\ 0 & \frac{1}{N}\left(\mathrm{e}^{i\frac{2\pi}{N}\sigma_1(k-1)} - 1\right) \end{bmatrix}. \tag{74}$$

We see that to first-order the contributions of the long-range links are independent from one another. In other words, to first-order, the contribution of all the links to the dynamics of mode k is the sum of the contributions of the individual links. To obtain the modal coordinate transformation (27) up to first-order we solve (45) with the matrices

$$\mathbf{A}_{k\ell}^{(1)} = \begin{bmatrix} 0 & 1 & -p\eta_{\ell 1} & 0 \\ p\eta_{k1} & \beta_1\eta_{k1} - \alpha & 0 & -p\eta_{\ell 1} \\ -1 & 0 & -\beta_1\eta_{\ell 1} + \alpha & 1 \\ 0 & -1 & p\eta_{k1} & \beta_1\eta_{k\ell} \end{bmatrix}, \tag{75}$$

and

$$\mathbf{c}_{k\ell}^{(1)} = \begin{bmatrix} 0 \\ 0 \\ 0 \\ \frac{1}{N}\mathrm{e}^{i\frac{2\pi}{N}(i_1-1)(\ell-k)}(\mathrm{e}^{i\frac{2\pi}{N}\sigma_1(\ell-1)} - 1)(\delta_{k\ell} - 1) \end{bmatrix}, \tag{76}$$

to obtain

$$\mathbf{b}_{k\ell}^{(1)} = \begin{bmatrix} u_{k\ell,11}^{(1)} \\ u_{k\ell,21}^{(1)} \\ u_{k\ell,12}^{(1)} \\ u_{k\ell,22}^{(1)} \end{bmatrix} = \frac{(1-\delta_{k\ell})(\mathrm{e}^{i\frac{2\pi}{N}\sigma_1(\ell-1)}-1)\mathrm{e}^{i\frac{2\pi}{N}(i_1-1)(\ell-k)}}{N\eta_{k\ell}(p-\alpha\beta_1)} \begin{bmatrix} \beta_1\eta_{\ell 1} \\ -p\eta_{\ell 1} \\ -1 \\ \alpha \end{bmatrix}. \tag{77}$$

Thus, a second-order approximation accounts for the interactions between the long-range links.

To get the second-order terms for the modal coordinate transformation (27) we solve (59) with matrices

$$\mathbf{A}_{k\ell}^{(1,2)} = \begin{bmatrix} 0 & 1 & -p\eta_{\ell 1} & 0 \\ p\eta_{k1} & \beta_1\eta_{k1}-\alpha & 0 & -p\eta_{\ell 1} \\ -1 & 0 & -\beta_1\eta_{\ell 1}+\alpha & 1 \\ 0 & -1 & p\eta_{k1} & \beta_1\eta_{k\ell} \end{bmatrix}, \tag{80}$$

and

$$\mathbf{c}_{k\ell}^{(1,2)} = \frac{2}{N} \begin{bmatrix} 0 \\ -\sum_{j=1}^{N} \mathrm{e}^{i\frac{2\pi}{N}(i_1-1)(j-k)}(\mathrm{e}^{i\frac{2\pi}{N}\sigma_1(j-1)}-1)u_{j\ell,21}^{(2)} \\ u_{k\ell,12}^{(1)}(\mathrm{e}^{i\frac{2\pi}{N}\sigma_2(\ell-1)}-1) \\ u_{k\ell,22}^{(1)}(\mathrm{e}^{i\frac{2\pi}{N}\sigma_2(\ell-1)}-1) - \sum_{j=1}^{N} \mathrm{e}^{i\frac{2\pi}{N}(i_1-1)(j-k)}(\mathrm{e}^{i\frac{2\pi}{N}\sigma_1(j-1)}-1)u_{j\ell,22}^{(2)} \end{bmatrix}, \tag{81}$$

Using the first-order perturbations upon $\hat{\mathbf{T}}$ we can obtain the second-order perturbation on the dynamics of mode k with respect to any two long-range links described by the indices $i_1, \sigma_1, i_2, \sigma_2$. In particular, (54) yields

$$[\hat{\mathbf{D}}^{(1,2)}]_k^k = [\hat{\mathbf{D}}_2(i_1,\sigma_1,i_2,\sigma_2)]_k^k = \begin{bmatrix} 0 & 0 \\ -2K_0(i_1,\sigma_1,i_2,\sigma_2) & -2K_1(i_1,\sigma_1,i_2,\sigma_2) \end{bmatrix}, \tag{78}$$

where

$$K_0(i_1,\sigma_1,i_2,\sigma_2) = \frac{p\eta_{k1}}{N^2(p-\alpha\beta_1)} \sum_{j=1,j\neq k}^{N} \frac{(\mathrm{e}^{i\frac{2\pi}{N}\sigma_1(j-1)}-1)(\mathrm{e}^{i\frac{2\pi}{N}\sigma_2(k-1)}-1)\mathrm{e}^{i\frac{2\pi}{N}(i_1-i_2)(j-k)}}{\eta_{jk}},$$

$$K_1(i_1,\sigma_1,i_2,\sigma_2) = \frac{-\alpha}{N^2(p-\alpha\beta_1)} \sum_{j=1,j\neq k}^{N} \frac{(\mathrm{e}^{i\frac{2\pi}{N}\sigma_1(j-1)}-1)(\mathrm{e}^{i\frac{2\pi}{N}\sigma_2(k-1)}-1)\mathrm{e}^{i\frac{2\pi}{N}(i_1-i_2)(j-k)}}{\eta_{jk}}. \tag{79}$$

Note that the second-order terms for two different links will depend on the parameters α, β_1, p, the indices of receiving cars (i_1, i_2), and the link lengths (σ_1, σ_2). where $u_{k\ell,\cdot\cdot}^{(1)}$ represent the elements of the 2×2 block $[\hat{\mathbf{U}}^{(1)}]_\ell^k$ are given by (77). The solution for the $\mathbf{b}_{k\ell}^{(1,2)}$ is given in "Appendix 2."

Using the elements of $\mathbf{b}_{k\ell}^{(1,2)}$ [cf. (94)] we can obtain the third-order perturbations of the dynamics due to any three long-range links defined by the indices $i_1, \sigma_1, i_2, \sigma_2, i_3, \sigma_3$ as

$$[\hat{\mathbf{D}}^{(1,2,3)}]_k^k = [\hat{\mathbf{D}}_3(i_1,\sigma_1,i_2,\sigma_2,i_3,\sigma_3)]_k^k = \begin{bmatrix} 0 & 0 \\ -6L_0(i_1,\sigma_1,i_2,\sigma_2,i_3,\sigma_3) & -6L_1(i_1,\sigma_1,i_2,\sigma_2,i_3,\sigma_3) \end{bmatrix}, \tag{82}$$

where $L_0(i_1,\sigma_1,i_2,\sigma_2,i_3,\sigma_3)$ and $L_1(i_1,\sigma_1,i_2,\sigma_2,i_3,\sigma_3)$ are given in "Appendix 3" [see (97)]. Thus, based on (64) the dynamics for mode k approximated up to third-order in $\beta_{i\sigma}$ become

$$\begin{aligned} \dot{\mathbf{z}}_k = &\left(\begin{bmatrix} 0 & 1 \\ p\eta_{k1} & \beta_1\eta_{k1}-\alpha \end{bmatrix} \right. \\ &+ \frac{1}{N} \sum_{i_1=1}^{N} \sum_{\sigma_1=2}^{\sigma_{\max}} \begin{bmatrix} 0 & 0 \\ 0 & (\mathrm{e}^{i\frac{2\pi}{N}\sigma_1(k-1)}-1) \end{bmatrix} \beta_{i_1\sigma_1} \\ &+ \sum_{i_1,i_2=1}^{N} \sum_{\sigma_1,\sigma_2=2}^{\sigma_{\max}} \begin{bmatrix} 0 & 0 \\ -K_0(i_1,\sigma_1,i_2,\sigma_2) & -K_1(i_1,\sigma_1,i_2,\sigma_2) \end{bmatrix} \\ &\beta_{i_1\sigma_1}\beta_{i_2\sigma_2} \\ &+ \sum_{i_1,i_2,i_3=1}^{N} \sum_{\sigma_1,\sigma_2,\sigma_3=2}^{\sigma_{\max}} \end{aligned}$$

$$\begin{bmatrix} 0 & 0 \\ -L_0(i_1,\sigma_1,i_2,\sigma_2,i_3,\sigma_3) & -L_1(i_1,\sigma_1,i_2,\sigma_2,i_3,\sigma_3) \end{bmatrix} \beta_{i_1\sigma_1}\beta_{i_2\sigma_2}\beta_{i_3\sigma_3}\Big)\mathbf{z}_k, \tag{83}$$

where the coefficients for the second- and third-order terms are given in (79) and (97), respectively.

To analyze the stability the modes we use the trial solution $\mathbf{z}_k(t) = \mathbf{z}_{k\,0}\mathrm{e}^{\lambda t}$ with $\mathbf{z}_{k\,0} \in \mathbb{C}^2$ and $\lambda \in \mathbb{C}$ for mode k. Thus, (83) yield the characteristic equation for

$$\begin{aligned}
\lambda^2 + \Bigg(&- \beta_1\eta_{k1} + \alpha + \frac{1}{N}\sum_{i_1=1}^{N}\sum_{\sigma_1=2}^{\sigma_{\max}}(1-\mathrm{e}^{i\frac{2\pi}{N}\sigma_1(k-1)})\beta_{i_1\sigma_1} \\
&+ \sum_{i_1,i_2=1}^{N}\sum_{\sigma_1,\sigma_2=2}^{\sigma_{\max}} K_1(i_1,\sigma_1,i_2,\sigma_2)\beta_{i_1\sigma_1}\beta_{i_2\sigma_2} \\
&+ \sum_{i_1,i_2,i_3=1}^{N}\sum_{\sigma_1,\sigma_2,\sigma_3=2}^{\sigma_{\max}} \\
&L_1(i_1,\sigma_1,i_2,\sigma_2,i_3,\sigma_3)\beta_{i_1\sigma_1}\beta_{i_2\sigma_2}\beta_{i_3\sigma_3}\Bigg)\lambda \\
+ \Bigg(&- p\eta_{k1} + \sum_{i_1,i_2=1}^{N}\sum_{\sigma_1,\sigma_2=2}^{\sigma_{\max}} K_0(i_1,\sigma_1,i_2,\sigma_2)\beta_{i_1\sigma_1}\beta_{i_2\sigma_2} \\
&+ \sum_{i_1,i_2,i_3=1}^{N}\sum_{\sigma_1,\sigma_2,\sigma_3=2}^{\sigma_{\max}} \\
&L_0(i_1,\sigma_1,i_2,\sigma_2,i_3,\sigma_3)\beta_{i_1\sigma_1}\beta_{i_2\sigma_2}\beta_{i_3\sigma_3}\Bigg) = 0.
\end{aligned} \tag{84}$$

We examine the stability of the connected vehicle network and its modes with respect to the equilibrium headway h^*. By considering the critical case $\lambda = i\omega$ we calculate the critical value of p_k using (84) which results in the corresponding headway h_k^* using (2,5) and determine the corresponding frequency ω_k. As both p_k and ω_k depend on the gains $\beta_{i\sigma}$ and we write these as expansions in $\beta_{i\sigma}$ up to third-order as

$$\begin{aligned}
p_k = p_{k0} &+ \sum_{i_1=1}^{N}\sum_{\sigma_1=2}^{\sigma_{\max}} p_{k1}(i_1,\sigma_1)\beta_{i_1\sigma_1} \\
&+ \frac{1}{2}\sum_{i_1,i_2=1}^{N}\sum_{\sigma_1,\sigma_2=2}^{\sigma_{\max}} p_{k2}(i_1,\sigma_1,i_2,\sigma_2)\beta_{i_1\sigma_1}\beta_{i_2\sigma_2} \\
&+ \frac{1}{6}\sum_{i_1,i_2,i_3=1}^{N}\sum_{\sigma_1,\sigma_2,\sigma_3=2}^{\sigma_{\max}} \\
&p_{k3}(i_1,\sigma_1,i_2,\sigma_2,i_3,\sigma_3)\beta_{i_1\sigma_1}\beta_{i_2\sigma_2}\beta_{i_3\sigma_3} + \cdots,
\end{aligned} \tag{85}$$

and

$$\begin{aligned}
\omega_k = \omega_{k0} &+ \sum_{i_1=1}^{N}\sum_{\sigma_1=2}^{\sigma_{\max}} \omega_{k1}(i_1,\sigma_1)\beta_{i_1\sigma_1} \\
&+ \frac{1}{2}\sum_{i_1,i_2=1}^{N}\sum_{\sigma_1,\sigma_2=2}^{\sigma_{\max}} \omega_{k2}(i_1,\sigma_1,i_2,\sigma_2)\beta_{i_1\sigma_1}\beta_{i_2\sigma_2} \\
&+ \frac{1}{6}\sum_{i_1,i_2,i_3=1}^{N}\sum_{\sigma_1,\sigma_2,\sigma_3=2}^{\sigma_{\max}} \\
&\omega_{k3}(i_1,\sigma_1,i_2,\sigma_2,i_3,\sigma_3)\beta_{i_1\sigma_1}\beta_{i_2\sigma_2}\beta_{i_3\sigma_3} + \cdots.
\end{aligned} \tag{86}$$

To obtain the coefficients in (85) and (86), we substitute them into (84), differentiate the result with respect to the $\beta_{i\sigma}$, evaluate the results at $\beta_{i\sigma} = 0$ and solve the two resulting algebraic equations for the terms of p_k and ω_k. The corresponding details are given in "Appendix 4."

The approximation to the stability boundary above can be used to directly determine the values of h_k^* at which stability is lost for mode k. Alternatively, given an equilibrium headway h^* one can find the set of gains to guarantee the linear stability of all modes.

4.3 Stability diagrams

In this subsection we visualize the results presented in the previous subsection using stability charts for connected vehicle networks with different connectivity structures. We plot the analytical approximations of the modal stability boundaries derived above and validate these results using numerical continuation. We consider long-range V2V links of length 2, 3 and 4. For simplicity, we assume that links of the same length use the same gain, i.e.,

$$\beta_{i2} = \beta_2, \quad \beta_{i3} = \beta_3, \quad \beta_{i4} = \beta_4. \tag{87}$$

We use the range policy (2) with $h_{\mathrm{st}} = 5\,[\mathrm{m}]$, $h_{\mathrm{go}} = 35\,[\mathrm{m}]$, and $v_{\max} = 30\,[\frac{\mathrm{m}}{\mathrm{s}}]$.

We first examine the effect of a single long-range link on the stability of connected vehicle networks. When vehicle $i = 1$ is receiving information through a link of length σ, as depicted in Fig. 3a1–c1, the linearized dynamics is described by (14) with matrix

$$\hat{\mathbf{J}} = \hat{\mathbf{J}}_0 + \hat{\mathbf{P}}(1,\sigma)\beta_\sigma, \tag{88}$$

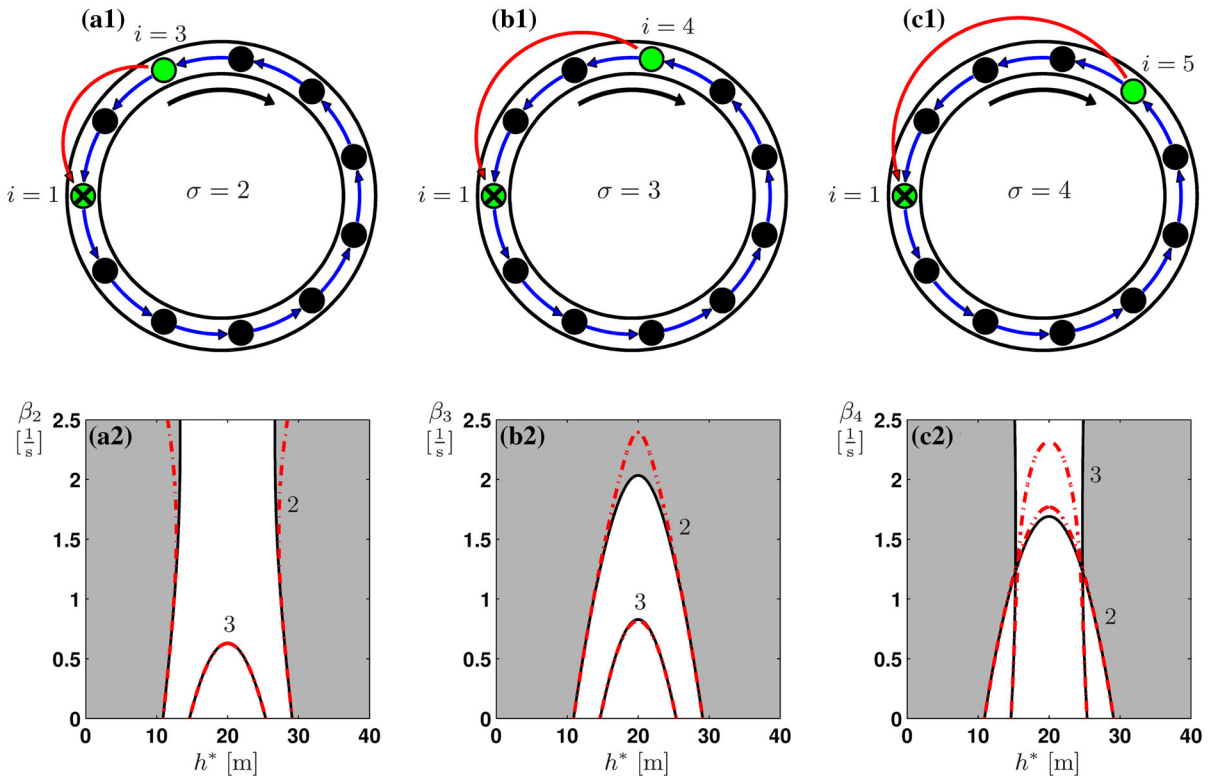

Fig. 3 *Top row* Diagrams of the vehicle configurations with a long-range V2V link for different link lengths for 11 cars. *Bottom row* Corresponding stability charts in the (h^*, β_σ) plane when considering $\beta_1 = 0.3\,[\frac{1}{s}]$ and $\alpha = 1\,[\frac{1}{s}]$. The *red dashed curves* denote the stability boundaries for the modes 2 and 3 obtained through the derived analytical approximation up to third-order in β_σ, while the *black solid curves* denote the linear stability boundaries obtained by numerical continuation. The *gray shaded* region corresponds to stable uniform flow. (Color figure online)

cf. (15) where $\varepsilon_{1\sigma} = \beta_\sigma$ is the gain for the link of length σ terminated at vehicle 1.

We first analyze the effect of link of length $\sigma = 2$ on the modal stability boundaries in the (h^*, β_2) plane for various values of α and β_1. The results are summarized in Fig. 4. The dashed red curves represent the analytical approximations of the modal stability boundaries up to third-order in β_2, while the solid black curves denote the boundaries obtained through numerical continuation [26]. Gray shading denotes stable uniform flow. The corresponding mode numbers k are shown next to each boundary. Only modes corresponding to $k = 2 \ldots \lfloor \frac{N}{2} + 1 \rfloor$ are shown, since modes k and $N + 2 - k$ are complex conjugates and therefore correspond to the same set of stability boundaries. The instability region for each mode is confined between the modal boundaries of that mode. Although the exact boundaries may cross each other (see Fig. 4a), the stability for the connected vehicle network is always given by mode 2 for the cases examined here.

Figure 4a contains four stability boundaries $k = 2, \ldots, 6$. When increasing β_2, the instability region for each mode shrinks and the uniform flow becomes stable for a wider range of h^*. As β_2 increases further some modal stability boundaries ($k = 3$ and 5) fold back, increasing the corresponding regions of instability. However, the $k = 2$ stability boundary (that gives the primary instability) is nearly vertical, so changing β_2 does not change the stability region significantly. As we increase the values of α and β_1 (going down and to the right in Fig. 4), stability boundaries for higher mode numbers disappear, and the range of h^* for which the system is stable increases. In fact, in Fig. 4f, h, k the connected vehicle network can be completely stabilized for a large enough gain β_2. Notice that the analytical approximations for the modal boundaries become more accurate for larger values of α and β_1 due to stronger cyclically symmetrical coupling.

Next we consider the effect of varying the length of the long-range link. In Fig. 3 we compare the linear sta-

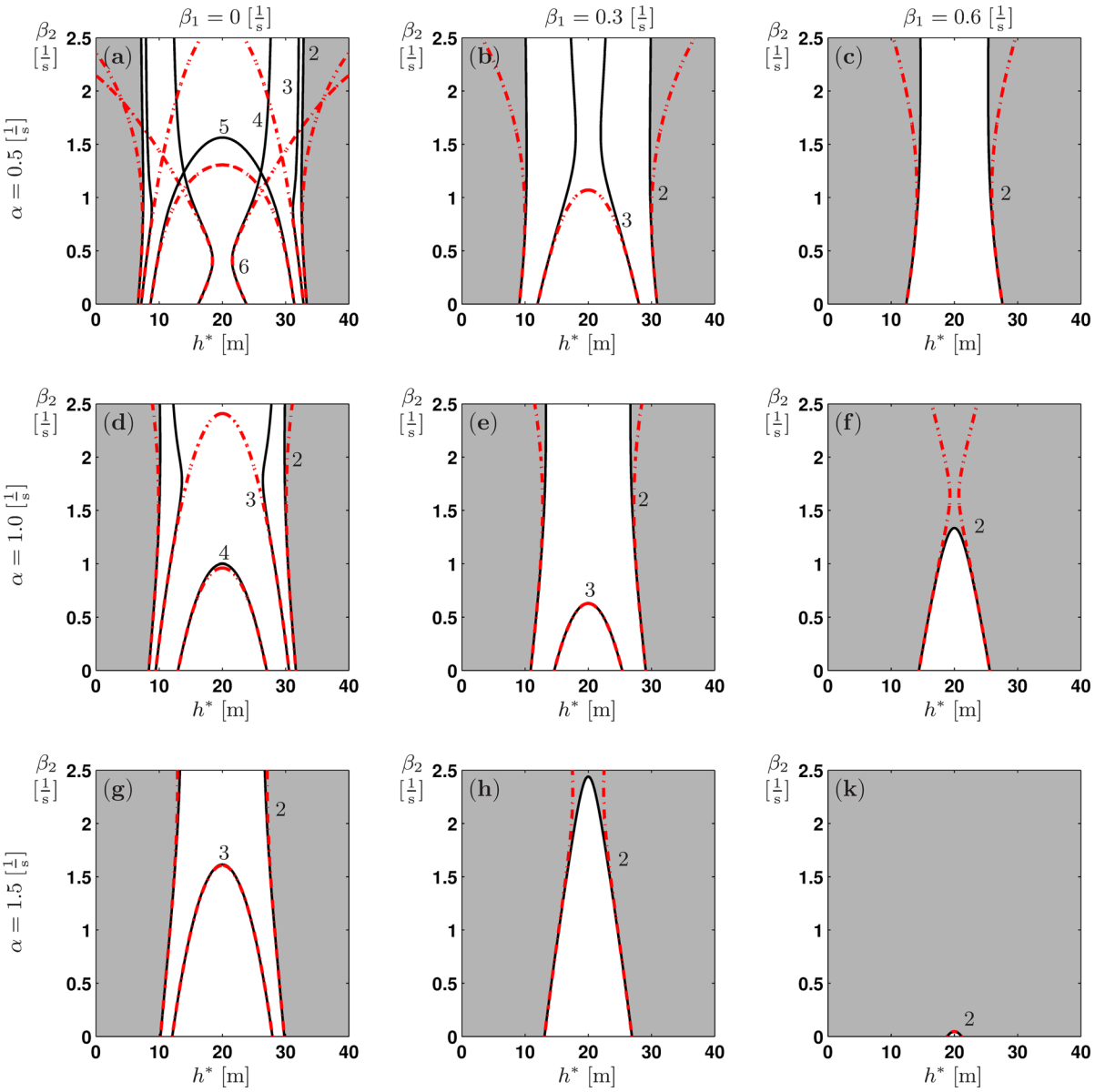

Fig. 4 Stability charts in the (h^*, β_2) plane when a V2V link of length 2 is added to an 11-car network. The β_1 and α values are indicated at each panel. The *red dashed curves* denote the stability boundaries for the modes $k = 2, \ldots, 6$ obtained through analytical approximation up to third-order in β_σ. The *black solid curves* denote the linear stability boundaries for modes obtained by numerical continuation. The *gray shaded* region corresponds to stable uniform flow. (Color figure online)

bility charts when a long-range link of length $\sigma = 2$, $\sigma = 3$, $\sigma = 4$ is added to an 11-car network. The configurations are depicted in Fig. 3a1, b1, c1, respectively, where the corresponding stability boundaries are shown in Fig. 3a2, b2, c2. In the case of $\sigma = 3$, increasing the gain β_σ corresponding to V2V link improves the stability (still determined by mode 2) more than in the case of $\sigma = 2$. In fact, a sufficiently large gain β_3 can be used to stabilize the uniform flow for all values of h^*. However, increasing β_3 has a smaller effect on the stability of mode 3 than increasing β_2, and it takes a larger value of β_3 to stabilize mode 3 for all values of h^*. In the case of $\sigma = 4$ increasing β_4 benefits the stability of the network for low values of β_4 where the

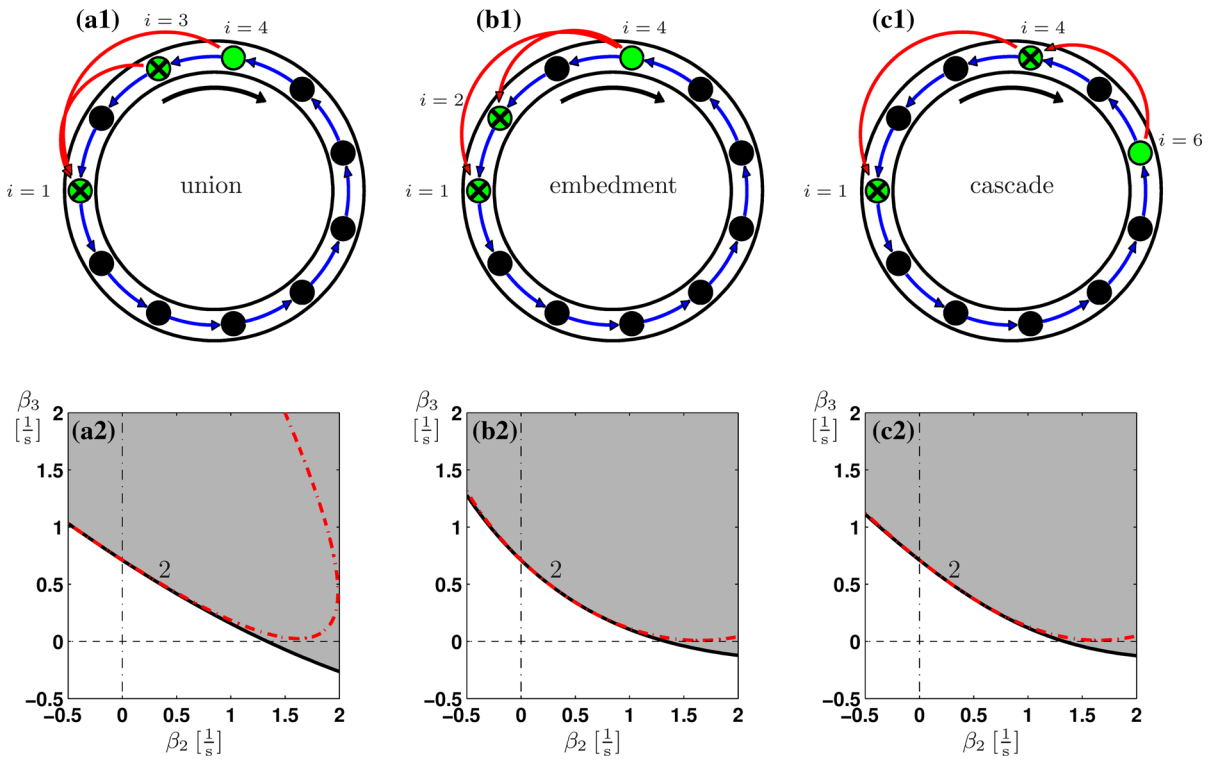

Fig. 5 *Top row* Connected vehicle networks with 11 cars and links of length 2 and 3 arranged in different configurations. *Bottom row* Stability charts in the (β_2, β_3) plane for $h^* = 20$ [m], $\beta_1 = 0.6$ $[\frac{1}{s}]$, and $\alpha = 1$ $[\frac{1}{s}]$. The same notation is used as in Fig. 3

stability boundary is given by mode 2. However, for $\beta_4 \gtrsim 1.23$ [1/s] the stability of the network is governed by mode 3, and increasing β_4 further has limited impact on the stability of the network.

After examining the effects of individual V2V links on stability of connected vehicle networks, we analyze the effects of combinations of these links. We first consider the scenario when the connected vehicle network contains two V2V links of different lengths ($\sigma = 2$ and $\sigma = 3$) and examine the stability for different configurations. A detailed description of different configurations can be found in [32], while examples of such combinations for an 11-car network are given at the top of Fig. 5. In the union configuration shown in Fig. 5a1 a single CCC vehicle ($i = 1$) utilizes information from multiple vehicles ahead ($i = 3$ and $i = 4$). In the embedment configuration depicted in Fig. 5b1 two distinct CCC vehicles ($i = 1$ and $i = 2$) utilize information from a single transmitting vehicle ($i = 4$). In the cascade configuration shown in Fig. 5c1, a CCC vehicle ($i = 1$) utilizes information from a connected vehicle ahead ($i = 4$), which also utilizes information from a vehicle further ahead ($i = 6$). The bottom row of Fig. 5 shows the stability charts for the three configurations in the (β_2, β_3) plane. The regions of stability for the three different configurations are similar, but the stability boundaries for the embedment and cascade cases are more concave. This indicates that the cascade and embedment configurations may have a greater benefit on the stability of the network than the "sum" of the individual links in these configurations.

After analyzing the typical configurations appearing in connected vehicle networks, we use the methodology outlined in Fig. 1 to construct a connected vehicle network for a ring with 33 cars. We setup the network as explained in Fig. 1b–e by first randomly selecting the transmitting vehicles with a probability of 0.5 and then randomly selecting the CCC vehicles with a probability of 0.5 out of the transmitting vehicles. Two of such connected vehicle networks are shown in Fig. 6a1, b1, labeled by "Trial 1" and "Trial 2". In both cases combinations of unions, embedment and cascades appear. Figure 6a2–b2 shows stability charts for the two trials in the (β_2, β_3) plane for different values of β_4. In Fig.

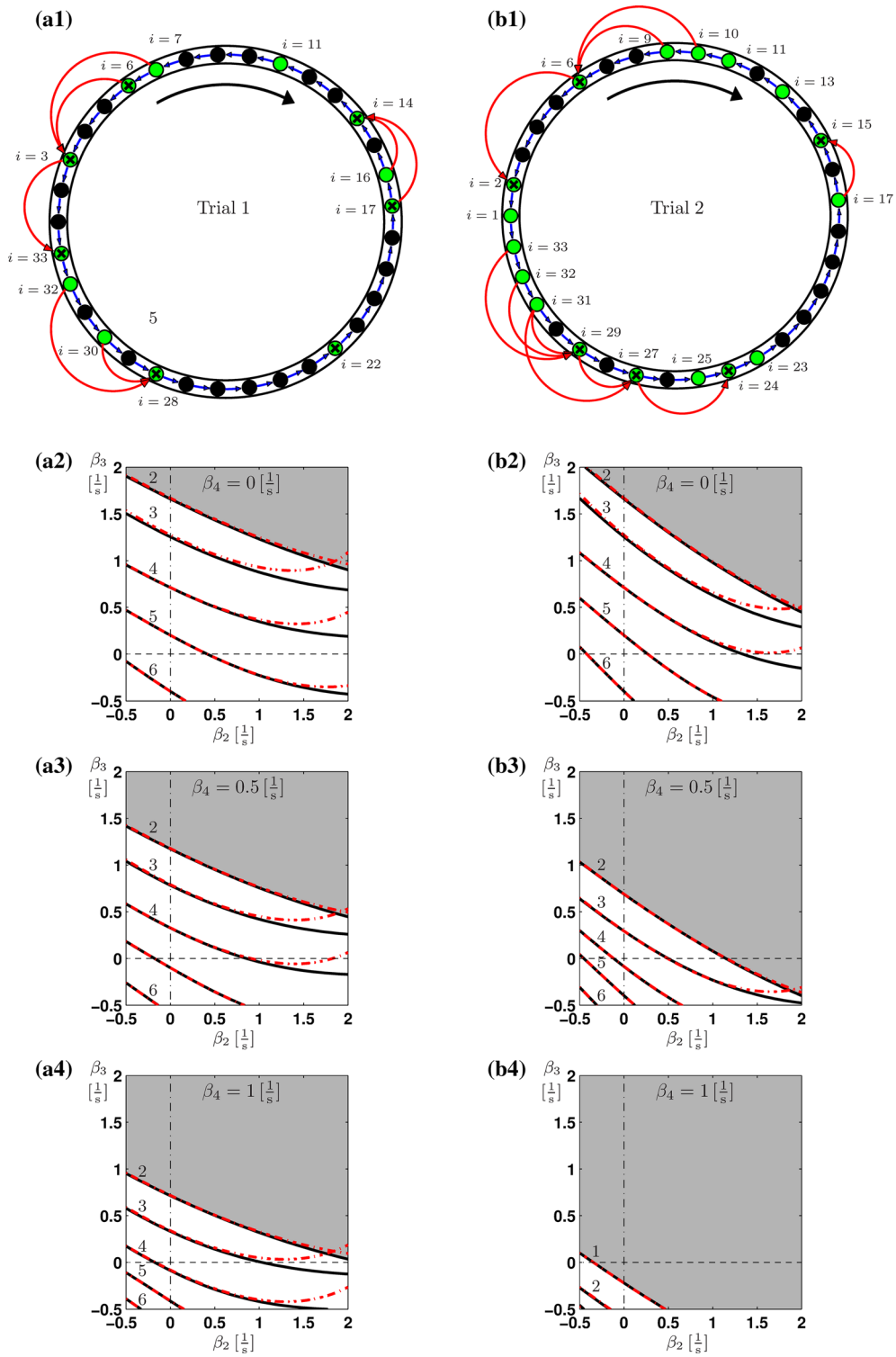

Fig. 6 **a1**, **b1** Two connected vehicle networks with 33 vehicles. **a2–a4**, **b2–b4** Corresponding stability charts in the (β_2, β_3) plane corresponding to for $h^* = 20\,[\mathrm{m}]$, $\alpha = 1\,[1/\mathrm{s}]$, $\beta_1 = 0.6\,[1/\mathrm{s}]$, and various values of β_4 as indicated. The same notation is used as in Fig. 3

6a2, b2, we have $\beta_4 = 0$, and stability boundaries for modes 2 through 6 appear. Note that the origin denotes the case of no V2V communication where modes 2 through 5 are unstable. Observe that the uniform flow can be stabilized by selecting sufficiently large gains β_2 and β_3. As β_4 is increased, the modal stability boundaries move down, and the network can be stabilized using smaller values of β_2 and β_3. In Fig. 6b4 only stability boundaries for modes 2 through 4 are present. Furthermore, Fig. 6b4 demonstrates that uniform flow can be stabilized only by using links of length 4, since the origin is located in the region of stable uniform flow.

5 Conclusion

In this paper we analyzed the dynamics of heterogeneous connected vehicle networks consisting of conventional vehicles that respond to the vehicle immediately ahead and vehicles equipped with connected cruise control (CCC) that use wireless vehicle-to-vehicle communication to respond to multiple vehicles ahead.

The nontrivial connectivity structure of such connected vehicle networks (CVNs) motivated us to develop a perturbation technique to approximate the modal dynamics of networks with heterogeneous connectivity by perturbing the modes of a corresponding cyclically symmetric network. First, the modal dynamics of the underlying cyclically symmetric network were determined through a discrete Fourier transformation. Subsequently the approximations to the modes of the heterogeneous network were obtained about the symmetric state. These expansions were obtained using linear algebraic equations that were decoupled by exploiting the symmetry of the underlying cyclically symmetric network. Specifically for a system with N nodes and M equations per node this reduction allows one to solve N^2 decoupled linear systems of M^2 unknowns instead of solving a single linear system with $(NM)^2$ unknowns. Furthermore, the resulting N^2 decoupled linear systems hare similar structure, which allows one to algorithmize the solution for increased efficiency.

This modal approximation technique was applied to heterogeneous connected vehicle systems including CCC vehicles which can also react to the velocity of up to four vehicles ahead. We first obtained the modal dynamics of the cyclically symmetric system containing no CCC vehicles. To obtain approximations of the modal equations when the connected vehicle network contains CCC vehicles, we calculated the modal expansions around the symmetric modes up to third-order in the V2V link gains. Using the obtained approximations we were able to analytically determine the modal stability boundaries for the heterogeneous connected vehicle networks. We validated the results by comparing these analytical boundaries to those obtained by numerical continuation.

We conclude that adding CCC vehicles to a vehicle network of human driven vehicles may stabilize the uniform flow. We observed that longer V2V links are more effective at stabilizing modes of low wave numbers, and less effective at stabilizing modes of high wave numbers. When adding multiple V2V links to a vehicle network, specific combinations of V2V links may enhance the impacts of the individual links on the stability of uniform flow. Finally, we demonstrated that in a large CVN having a few appropriately designed V2V links may be adequate to stabilize the uniform flow.

We found the network-based modal approximation technique to be effective in analyzing the linear stability of large connected vehicle networks with heterogeneous connectivity. In the future we will use this technique to evaluate the effects of increasing connected vehicle penetration on the stability of uniform flow. Furthermore, we will use numerical simulations in order to evaluate the behavior of CVNs at the nonlinear level. In the long term we will seek to implement the developed techniques as a part of a larger algorithm that would enable one to analyze more complex and more realistic connected vehicle networks.

Acknowledgements Funding was provided by the National Science Foundation (Award No. 1351456).

Appendix 1: Third-order approximation of modal dynamics

To obtain the third-order perturbation of the dynamics of the k-th mode $[\hat{\mathbf{D}}^{(1,2,3)}]_k^k$ for an arbitrary $i_1, \sigma_1, i_2, \sigma_2, i_3, \sigma_3$ sextuple we take the derivative of (49) with respect to $\varepsilon_{i_3\sigma_3}$ (denoted by ε_3) which yields

$$\partial_{\varepsilon_1}\partial_{\varepsilon_2}\partial_{\varepsilon_3}\left(\hat{\mathbf{J}} - \mathbf{I}_N \otimes [\hat{\mathbf{D}}]_k^k\right)[\hat{\mathbf{T}}]_k + \partial_{\varepsilon_1}\partial_{\varepsilon_2}\left(\hat{\mathbf{J}} - \mathbf{I}_N \otimes [\hat{\mathbf{D}}]_k^k\right)\partial_{\varepsilon_3}[\hat{\mathbf{T}}]_k$$

$$
\begin{aligned}
&+\partial_{\varepsilon_1}\partial_{\varepsilon_3}\left(\hat{\mathbf{J}}-\mathbf{I}_N\otimes[\hat{\mathbf{D}}]_k^k\right)\partial_{\varepsilon_2}[\hat{\mathbf{T}}]_k\\
&+\partial_{\varepsilon_2}\partial_{\varepsilon_3}\left(\hat{\mathbf{J}}-\mathbf{I}_N\otimes[\hat{\mathbf{D}}]_k^k\right)\partial_{\varepsilon_1}[\hat{\mathbf{T}}]_k\\
&+\partial_{\varepsilon_1}\left(\hat{\mathbf{J}}-\mathbf{I}_N\otimes[\hat{\mathbf{D}}]_k^k\right)\partial_{\varepsilon_2}\partial_{\varepsilon_3}[\hat{\mathbf{T}}]_k\\
&+\partial_{\varepsilon_2}\left(\hat{\mathbf{J}}-\mathbf{I}_N\otimes[\hat{\mathbf{D}}]_k^k\right)\partial_{\varepsilon_1}\partial_{\varepsilon_3}[\hat{\mathbf{T}}]_k\\
&+\partial_{\varepsilon_3}\left(\hat{\mathbf{J}}-\mathbf{I}_N\otimes[\hat{\mathbf{D}}]_k^k\right)\partial_{\varepsilon_1}\partial_{\varepsilon_2}[\hat{\mathbf{T}}]_k\\
&+\left(\hat{\mathbf{J}}-\mathbf{I}_N\otimes[\hat{\mathbf{D}}]_k^k\right)\partial_{\varepsilon_1}\partial_{\varepsilon_2}\partial_{\varepsilon_3}[\hat{\mathbf{T}}]_k=0. \qquad (89)
\end{aligned}
$$

At $\varepsilon_{i_1\sigma_1}=\varepsilon_{i_2\sigma_2}=\varepsilon_{i_3\sigma_3}=0$ we obtain

$$
\begin{aligned}
&\frac{1}{6}\mathbf{I}_N\otimes\Big([\hat{\mathbf{D}}^{(1,2,3)}]_k^k+[\hat{\mathbf{D}}^{(1,3,2)}]_k^k+[\hat{\mathbf{D}}^{(2,1,3)}]_k^k\\
&+[\hat{\mathbf{D}}^{(2,3,1)}]_k^k+[\hat{\mathbf{D}}^{(3,1,2)}]_k^k+[\hat{\mathbf{D}}^{(3,2,1)}]_k^k\Big)\\
&=-\frac{1}{2}\mathbf{I}_N\otimes\Big([\hat{\mathbf{D}}^{(1,2)}]_k^k+[\hat{\mathbf{D}}^{(2,1)}]_k^k\Big)[\hat{\mathbf{T}}^{(3)}]_k\\
&\quad-\frac{1}{2}\mathbf{I}_N\otimes\Big([\hat{\mathbf{D}}^{(1,3)}]_k^k+[\hat{\mathbf{D}}^{(3,1)}]_k^k\Big)[\hat{\mathbf{T}}^{(2)}]_k\\
&\quad-\frac{1}{2}\mathbf{I}_N\otimes\Big([\hat{\mathbf{D}}^{(2,3)}]_k^k+[\hat{\mathbf{D}}^{(3,2)}]_k^k\Big)[\hat{\mathbf{T}}^{(1)}]_k\\
&\quad+\frac{1}{2}(\hat{\mathbf{P}}^{(1)}-\mathbf{I}_N\otimes[\hat{\mathbf{D}}^{(1)}]_k^k)([\hat{\mathbf{T}}^{(2,3)}]_k+[\hat{\mathbf{T}}^{(3,2)}]_k)\\
&\quad+\frac{1}{2}(\hat{\mathbf{P}}^{(2)}-\mathbf{I}_N\otimes[\hat{\mathbf{D}}^{(2)}]_k^k)([\hat{\mathbf{T}}^{(1,3)}]_k+[\hat{\mathbf{T}}^{(3,1)}]_k)\\
&\quad+\frac{1}{2}(\hat{\mathbf{P}}^{(3)}-\mathbf{I}_N\otimes[\hat{\mathbf{D}}^{(3)}]_k^k)([\hat{\mathbf{T}}^{(1,2)}]_k+[\hat{\mathbf{T}}^{(2,1)}]_k)\\
&\quad+\frac{1}{6}(\hat{\mathbf{J}}_0-\mathbf{I}_N\otimes[\hat{\mathbf{D}}_0]_k^k)\Big([\hat{\mathbf{T}}^{(1,2,3)}]_k+[\hat{\mathbf{T}}^{(1,3,2)}]_k\\
&\quad+[\hat{\mathbf{T}}^{(2,1,3)}]_k+[\hat{\mathbf{T}}^{(2,3,1)}]_k+[\hat{\mathbf{T}}^{(3,1,2)}]_k\\
&\quad+[\hat{\mathbf{T}}^{(3,2,1)}]_k\Big). \qquad (90)
\end{aligned}
$$

We can eliminate the last term in the expression above by multiplying by $[\hat{\mathbf{T}}_0^{-1}]^k$ from the left and using (26). Also because the above expression has six unknowns (the $[\hat{\mathbf{D}}^{(\cdot,\cdot,\cdot)}]_k^k$'s) for each i_1, σ_1, i_2, σ_2, i_3, σ_3 sextuple we have the freedom to set

$$
\begin{aligned}
[\hat{\mathbf{D}}^{(1,2,3)}]_k^k&=[\hat{\mathbf{D}}_3(i_1,\sigma_1,i_2,\sigma_2,i_3,\sigma_3)]_k^k\\
&=-3[\hat{\mathbf{T}}_0^{-1}]^k(\mathbf{I}_N\otimes[\hat{\mathbf{D}}^{(1,2)}]_k^k)\hat{\mathbf{T}}_0[\hat{\mathbf{U}}^{(3)}]_k\\
&\quad+3[\hat{\mathbf{T}}_0^{-1}]^k(\hat{\mathbf{P}}^{(1)}-\mathbf{I}_N\otimes[\hat{\mathbf{D}}^{(1)}]_k^k)\hat{\mathbf{T}}_0[\hat{\mathbf{U}}^{(2,3)}]_k, \qquad (91)
\end{aligned}
$$

while the equations for the other third-order terms can be obtained by permuting on the indices corresponding to i_1, σ_1, i_2, σ_2, i_3, σ_3 on the left and right hand side of (91). By algebraic manipulation one can show $[\hat{\mathbf{T}}_0^{-1}]^k(\mathbf{I}_N\otimes[\hat{\mathbf{D}}^{(1,2)}]_k^k)\hat{\mathbf{T}}_0[\hat{\mathbf{U}}^{(3)}]_k=[\hat{\mathbf{T}}_0^{-1}]^k(\mathbf{I}_N\otimes[\hat{\mathbf{D}}^{(1)}]_k^k)\hat{\mathbf{T}}_0[\hat{\mathbf{U}}^{(2,3)}]_k=0$. This means we can simplify (91) to

$$
[\hat{\mathbf{D}}^{(1,2,3)}]_k^k=3[\hat{\mathbf{T}}_0^{-1}]^k\hat{\mathbf{P}}^{(1)}\hat{\mathbf{T}}_0[\hat{\mathbf{U}}^{(2,3)}]_k, \qquad (92)
$$

and by using (17) we can obtain (62).

Appendix 2: Second-order approximation of the modal block eigenvector

Solving (59) for the connected vehicle network , we obtain the (k,ℓ)-th block of $\hat{\mathbf{U}}^{(1,2)}$ whose elements are contained in

$$
\mathbf{b}_{k\ell}^{(1,2)}=\begin{bmatrix}u_{k\ell,11}^{(1,2)}\\ u_{k\ell,21}^{(1,2)}\\ u_{k\ell,12}^{(1,2)}\\ u_{k\ell,22}^{(1,2)}\end{bmatrix}. \qquad (93)
$$

For $k\neq\ell$ using (80,81) we obtain

$$
\begin{aligned}
\mathbf{b}_{k\ell}^{(1,2)}&=\frac{1}{p(p-\alpha\beta_1)\eta_{k\,\ell}}\\
&\times\begin{bmatrix}(p+\beta_1(\beta_1\eta_{\ell 1}-\alpha))R(i_1,\sigma_1,i_2,\sigma_2)_{k\ell}+p\eta_{\ell 1}(p+\beta_1(\beta_1\eta_{k1}-\alpha))Q(i_1,\sigma_1,i_2,\sigma_2)_{k\ell}-p\beta_1\eta_{\ell 1}S(i_1,\sigma_1,i_2,\sigma_2)_{k\ell}\\ p\eta_{\ell 1}(-\beta_1R(i_1,\sigma_1,i_2,\sigma_2)_{k\ell}-p\beta_1\eta_{k1}Q(i_1,\sigma_1,i_2,\sigma_2)_{k\ell}+pS(i_1,\sigma_1,i_2,\sigma_2)_{k\ell})\\ (-p\beta_1\eta_{k1}Q(i_1,\sigma_1,i_2,\sigma_2)_{k\ell}-\beta_1R(i_1,\sigma_1,i_2,\sigma_2)_{k\ell}+pS(i_1,\sigma_1,i_2,\sigma_2)_{k\ell})\\ p(R(i_1,\sigma_1,i_2,\sigma_2)_{k\ell}+p\eta_{k1}Q(i_1,\sigma_1,i_2,\sigma_2)_{k\ell}-\alpha\,S(i_1,\sigma_1,i_2,\sigma_2)_{k\,\ell})\end{bmatrix}, \qquad (94)
\end{aligned}
$$

where

$$
\begin{aligned}
Q(i_1,\sigma_1,i_2,\sigma_2)_{k\,\ell} &= \frac{2}{N}u^{(1)}_{k\ell,12}\Big(\mathrm{e}^{i\frac{2\pi}{N}\sigma_2(\ell-1)}-1\Big),\\
R(i_1,\sigma_1,i_2,\sigma_2)_{k\,\ell} &= \frac{2}{N}\Bigg(-\sum_{j=1}^{N}\mathrm{e}^{i\frac{2\pi}{N}(i_1-1)(j-k)}\\
&\quad\times\Big(\mathrm{e}^{i\frac{2\pi}{N}\sigma_1(j-1)}-1\Big)u^{(2)}_{j\ell,21}\Bigg),\\
S(i_1,\sigma_1,i_2,\sigma_2)_{k\,\ell} &= \frac{2}{N}\Bigg(u^{(1)}_{k\ell,22}\Big(\mathrm{e}^{i\frac{2\pi}{N}\sigma_2(\ell-1)}-1\Big)\\
&\quad-\sum_{j=1}^{N}\mathrm{e}^{i\frac{2\pi}{N}(i_1-1)(j-k)}\\
&\quad\times\Big(\mathrm{e}^{i\frac{2\pi}{N}\sigma_1(j-1)}-1\Big)u^{(2)}_{j\ell,22}\Bigg).
\end{aligned}
\tag{95}
$$

and $u^{(1)}_{k\ell,12}$, $u^{(2)}_{j\ell,21}$, $u^{(1)}_{k\ell,22}$, $u^{(2)}_{j\ell,22}$ are given in (77). For the case $k=\ell$ (59) has multiple possible solutions due to a nonzero nullity. In this case, we set

$$
\mathbf{b}^{(1,2)}_{k\ell}=\begin{bmatrix}0\\0\\0\\0\end{bmatrix}. \tag{96}
$$

Appendix 3: Cubic terms of the modal approximation

The coefficients in (82) and (83) are given by

$$
\begin{aligned}
&L_0(i_1,\sigma_1,i_2,\sigma_2,i_3,\sigma_3)=\frac{1}{N^3}\frac{p\eta_{k1}}{(p-\alpha\beta_1)^2}\\
&\sum_{u=1,u\neq k}^{N}\frac{(\mathrm{e}^{i\frac{2\pi}{N}\sigma_1(u-1)}-1)\mathrm{e}^{i\frac{2\pi}{N}(i_1-1)(u-k)}}{\eta_{uk}}\\
&\times\Bigg(-\frac{(\mathrm{e}^{i\frac{2\pi}{N}\sigma_2(k-1)}-1)(\mathrm{e}^{i\frac{2\pi}{N}\sigma_3(k-1)}-1)\mathrm{e}^{i\frac{2\pi}{N}(i_2-1)(k-u)}}{\eta_{uk}}\\
&(\beta_1\eta_{u1}+\alpha)+\sum_{j=1,j\neq k}^{N}\\
&\frac{(\mathrm{e}^{i\frac{2\pi}{N}\sigma_2(j-1)}-1)(\mathrm{e}^{i\frac{2\pi}{N}\sigma_3(k-1)}-1)\mathrm{e}^{i\frac{2\pi}{N}(i_2-1)(j-u)}\mathrm{e}^{i\frac{2\pi}{N}(i_3-1)(k-j)}}{\eta_{jk}}\\
&(\beta_1\eta_{k1}+\alpha)\Bigg),
\end{aligned}
$$

and

$$
\begin{aligned}
&L_1(i_1,\sigma_1,i_2,\sigma_2,i_3,\sigma_3)=\frac{1}{N^3}\frac{1}{(p-\alpha\beta_1)^2}\\
&\sum_{u=1,u\neq k}^{N}\frac{(\mathrm{e}^{i\frac{2\pi}{N}\sigma_1(u-1)}-1)\mathrm{e}^{i\frac{2\pi}{N}(i_1-1)(u-k)}}{\eta_{uk}}\\
&\times\Bigg(\frac{(\mathrm{e}^{i\frac{2\pi}{N}\sigma_2(k-1)}-1)(\mathrm{e}^{i\frac{2\pi}{N}\sigma_3(k-1)}-1)\mathrm{e}^{i\frac{2\pi}{N}(i_2-1)(k-u)}}{\eta_{uk}}\\
&(p\eta_{u1}+\alpha^2)-\sum_{j=1,j\neq k}^{N}\\
&\frac{(\mathrm{e}^{i\frac{2\pi}{N}\sigma_2(j-1)}-1)(\mathrm{e}^{i\frac{2\pi}{N}\sigma_3(k-1)}-1)\mathrm{e}^{i\frac{2\pi}{N}(i_2-1)(j-u)}\mathrm{e}^{i\frac{2\pi}{N}(i_3-1)(k-j)}}{\eta_{jk}}\\
&(p\eta_{k1}+\alpha^2)\Bigg).
\end{aligned}
\tag{97}
$$

Appendix 4: Coefficients for modal stability boundaries and modal frequencies

The coefficients for p_k and ω_k in (85) and (86) are obtained by plugging in (85) and (86) into (84) with $p=p_k$ and $\lambda=i\omega_k$. The zeroth-order terms in (85) and (86) are then determined by setting all $\beta_{i\sigma}=0$, taking the real and imaginary parts of (84), and solving the resulting two equations for p_{k0} and ω_{k0} we obtain

$$
\begin{aligned}
p_{k0} &= \tfrac{1}{2}(2\beta_1+\alpha)\Big((2\beta_1+\alpha)\tan^2\Big(\tfrac{\theta_k}{2}\Big)+\alpha\Big),\\
\omega_{k0} &= (2\beta_1+\alpha)\tan\Big(\tfrac{\theta_k}{2}\Big),
\end{aligned}
\tag{98}
$$

where $\theta_k=\frac{2\pi}{N}(k-1)$. These expressions indeed correspond to (72) and (73).

To obtain the first-order terms for indices i_1,σ_1, we take the partial derivative of (84) with respect to $\beta_{i_1\sigma_1}$ and evaluate the expression at $\beta_{i_1\sigma_1}=0$. Then taking the real and imaginary parts, and performing some algebraic manipulation we get

$$
\begin{aligned}
p_{k1}(i_1,\sigma_1) &= \frac{1}{2N}\Bigg(\omega_{k0}\Bigg(\sin(\sigma_1\theta_k)+\frac{2\big(1+\sin\big(\frac{\theta_k}{2}\big)\big)}{\sin(\theta_k)}\\
&\quad\times\big(1-\cos(\sigma_1\theta_k)\big)\Bigg)\\
&\quad+\alpha\Bigg(\frac{\sin(\sigma_1\theta_k)}{\tan\big(\frac{\theta_k}{2}\big)}+\big(1-\cos(\sigma_1\theta_k)\big)\Bigg)\Bigg)\\
\omega_{k1}(i_1,\sigma_1) &= \frac{1}{N}\Bigg(\sin(\sigma_1\theta_k)+\tan(\tfrac{\theta_k}{2})\big(1-\cos(\sigma_1\theta_k)\big)\Bigg).
\end{aligned}
\tag{99}
$$

Similarly, the second-order terms for the indices $i_1,\sigma_1,i_2,\sigma_2$ can be obtained by taking the second partial derivative of (84) with respect to $\beta_{i_1\sigma_1}$ and $\beta_{i_2\sigma_2}$ and evaluating the results at $\beta_{i_1\sigma_1}=\beta_{i_2\sigma_2}=0$. Splitting the real and imaginary parts we obtain

$$
\begin{aligned}
p_{k2}(i_1,\sigma_1,i_2,\sigma_2) &= \frac{2}{N}\omega_{k1}(i_1,\sigma_1)_k\frac{1-\cos(\sigma_2\theta_k)}{\sin(\theta_k)}\\
&+\left(2\omega_{k0}\frac{1+\sin^2\left(\frac{\theta_k}{2}\right)}{\sin(\theta_k)}+\alpha\right)\Bigg(\mathrm{Re}\,K_1(i_1,\sigma_1,i_2,\sigma_2)|_{\mathrm{c}}\\
&+\frac{1}{\omega_{k0}}\mathrm{Im}\,K_0(i_1,\sigma_1,i_2,\sigma_2)|_{\mathrm{c}}\Bigg)\\
&+\left(\omega_{k0}+\alpha\frac{2\cos^2\left(\frac{\theta_k}{2}\right)}{\sin(\theta_k)}\right)\Bigg(-\mathrm{Im}K_1\,(i_1,\sigma_1,i_2,\sigma_2)|_{\mathrm{c}}\\
&+\frac{1}{\omega_{k0}}\mathrm{Re}\,K_0(i_1,\sigma_1,i_2,\sigma_2)|_{\mathrm{c}}\Bigg)\\
\omega_{k2}(i_1,\sigma_1,i_2,\sigma_2) &= 2\Bigg(\mathrm{Re}\,K_1(i_1,\sigma_1,i_2,\sigma_2)|_{\mathrm{c}}\tan\left(\tfrac{\theta_k}{2}\right)\\
&-\mathrm{Im}\,K_1(i_1,\sigma_1,i_2,\sigma_2)|_{\mathrm{c}}\Bigg)\\
&+\frac{2}{\omega_{k0}}\Bigg(\mathrm{Re}\,K_0(i_1,\sigma_1,i_2,\sigma_2)|_{\mathrm{c}}\\
&+\mathrm{Im}\,K_0(i_1,\sigma_1,i_2,\sigma_2)|_{\mathrm{c}}\tan\left(\tfrac{\theta_k}{2}\right)\Bigg),
\end{aligned}
\tag{100}
$$

where "$|_{\mathrm{c}}$" indicates that the quantity is evaluated with all $\beta_{i\sigma}=0$.

Finally, to obtain the third-order terms for the indices $i_1,\sigma_1,i_2,\sigma_2,i_3,\sigma_3$ we take the third partial derivative of (84) with respect to $\beta_{i_1\sigma_1}$, $\beta_{i_2\sigma_2}$, and $\beta_{i_3\sigma_3}$ and evaluate the result at $\beta_{i_1\sigma_1}=\beta_{i_2\sigma_2}=\beta_{i_3\sigma_3}=0$. Taking the real and imaginary parts yields

$$
\begin{aligned}
p_{k3}(i_1,\sigma_1,i_2,\sigma_2,i_3,\sigma_3) &= 3\omega_{k1}(i_1,\sigma_1)\omega_{k2}(i_1,\sigma_1,i_2,\sigma_2)\\
&+\frac{3}{N}\frac{1-\cos(\sigma_1\theta)}{\sin(\theta_k)}\omega_{k2}(i_2,\sigma_2,i_3,\sigma_3)\\
&+\left(\frac{3}{2}\omega_{k0}+\frac{\alpha}{2}\frac{1}{\tan\left(\frac{\theta_k}{2}\right)}\right)\omega_{k3}(i_1,\sigma_1,i_2,\sigma_2,i_3,\sigma_3)\\
&+6\omega_{k1}(i_1,\sigma_1)\Bigg(\mathrm{Re}\,K_1(i_2,\sigma_2,i_3,\sigma_3)|_{\mathrm{c}}\frac{1}{\tan(\theta_k)}\\
&+\mathrm{Im}\,K_1(i_2,\sigma_2,i_3,\sigma_3)|_{\mathrm{c}}\Bigg)\\
&+6\omega_{k0}\Bigg(\partial_{\varepsilon_1}\mathrm{Re}\,K_1(i_2,\sigma_2,i_3,\sigma_3)|_{\mathrm{c}}\frac{1}{\tan(\theta_k)}\\
&+\partial_{\varepsilon_1}\mathrm{Im}\,K_1(i_2,\sigma_2,i_3,\sigma_3)|_{\mathrm{c}}\Bigg)\\
&+6\omega_{k0}\Bigg(\mathrm{Re}\,L_1(i_1,\sigma_1,i_2,\sigma_2,i_3,\sigma_3)|_{\mathrm{c}}\frac{1}{\tan(\theta_k)}\\
&+\mathrm{Im}\,L_1(i_1,\sigma_1,i_2,\sigma_2,i_3,\sigma_3)|_{\mathrm{c}}\Bigg)\\
&+6\Bigg(\partial_{\varepsilon_1}\mathrm{Im}\,K_0(i_2,\sigma_2,i_3,\sigma_3)|_{\mathrm{c}}\frac{1}{\tan(\theta_k)}\\
&-\partial_{\varepsilon_1}\mathrm{Re}\,K_0(i_2,\sigma_2,i_3,\sigma_3)|_{\mathrm{c}}\Bigg)\\
&+6\Bigg(\mathrm{Im}\,L_0(i_1,\sigma_1,i_2,\sigma_2,i_3,\sigma_3)|_{\mathrm{c}}\frac{1}{\tan(\theta_k)}\\
&-\mathrm{Re}\,L_0(i_1,\sigma_1,i_2,\sigma_2,i_3,\sigma_3)|_{\mathrm{c}}\Bigg),\\
\omega_{k3}(i_1,\sigma_1,i_2,\sigma_2,i_3,\sigma_3) &= -3\frac{\omega_{k1}(i_1,\sigma_1)\omega_{k2}(i_2,\sigma_2,i_3,\sigma_3)}{\omega_{k0}}\\
&+6\frac{\omega_{k1}(i_1,\sigma_1)}{\omega_{k0}}\Bigg(\mathrm{Re}\,K_1(i_2,\sigma_2,i_3,\sigma_3)|_{\mathrm{c}}\tan\left(\tfrac{\theta_k}{2}\right)\\
&-\mathrm{Im}\,K_1(i_2,\sigma_2,i_3,\sigma_3)|_{\mathrm{c}}\Bigg)\\
&+6\Bigg(\partial_{\varepsilon_1}\mathrm{Re}\,K_1(i_2,\sigma_2,i_3,\sigma_3)|_{\mathrm{c}}\tan\left(\tfrac{\theta_k}{2}\right)\\
&-\partial_{\varepsilon_1}\mathrm{Im}\,K_1(i_2,\sigma_2,i_3,\sigma_3)|_{\mathrm{c}}\Bigg)\\
&+6\Bigg(\mathrm{Re}\,L_1(i_1,\sigma_1,i_2,\sigma_2,i_3,\sigma_3)|_{\mathrm{c}}\tan\left(\tfrac{\theta_k}{2}\right)\\
&-\mathrm{Im}\,L_1(i_1,\sigma_1,i_2,\sigma_2,i_3,\sigma_3)|_{\mathrm{c}}\Bigg)\\
&+\frac{6}{\omega_{k0}}\Bigg(\partial_{\varepsilon_1}\mathrm{Re}\,K_0(i_2,\sigma_2,i_3,\sigma_3)|_{\mathrm{c}}\\
&+\partial_{\varepsilon_1}\mathrm{Im}\,K_0(i_2,\sigma_2,i_3,\sigma_3)|_{\mathrm{c}}\tan(\tfrac{\theta_k}{2})\Bigg)\\
&+\frac{6}{\omega_{k0}}\Bigg(\mathrm{Re}\,L_0(i_1,\sigma_1,i_2,\sigma_2,i_3,\sigma_3)|_{\mathrm{c}}\\
&+\mathrm{Im}\,L_0(i_1,\sigma_1,i_2,\sigma_2,i_3,\sigma_3)|_{\mathrm{c}}\tan\left(\tfrac{\theta_k}{2}\right)\Bigg).
\end{aligned}
\tag{101}
$$

References

1. Alam, A., Mårtensson, J., Johansson, K.H.: Experimental evaluation of decentralized cooperative cruise control for heavy-duty vehicle platooning. Control Eng. Pract. **38**, 11–25 (2015)
2. Alam, A., Besselink, B., Turri, V., Martensson, J., Johansson, K.H.: Heavy-duty vehicle platooning for sustainable freight transportation: a cooperative method to enhance safety and efficiency. IEEE Control Syst. **35**(6), 34–56 (2015)
3. Avedisov, S.S., Orosz, G.: Nonlinear network modes in cyclic systems with applications to connected vehicles. J. Nonlinear Sci. **25**(4), 1015–1049 (2015)
4. di Bernardo, M., Salvi, A., Santini, S.: Distributed consensus strategy for platooning of vehicles in the presence of time-varying heterogeneous communication delays. IEEE Trans. Intell. Transp. Syst. **16**(1), 102–112 (2015)
5. Gallagher, B., Akatsuka, H., Suzuki, H.: Wireless communications for vehicle safety: radio link performance and wireless connectivity methods. IEEE Veh. Technol. Mag. **1**(4), 4–24 (2006)
6. Ge, J.I., Avedisov, S.S., Orosz, G.: Stability of connected vehicle platoons with delayed acceleration feedback. In: Proceedings of the ASME Dynamical Systems and Control Conference. ASME (2013). Paper no. DSCC2013-4040

7. Ge, J.I., Orosz, G.: Dynamics of connected vehicle systems with delayed acceleration feedback. Transp. Res. Part C Emerg. Technol. **46**, 46–64 (2014)
8. Ge, J.I., Orosz, G., Hajdu, D., Insperger, T., Moehlis, J.: To delay or not to delay—stability of connected cruise control time delay systems. Theory, numerics, applications, and experiments. In: Insperger, T., Ersal, T., Orosz, G. (eds.) Advances in Delays and Dynamics, vol. 7, pp. 263–282. Springer, Berlin (2017)
9. Ge, J.I., Orosz, G.: Optimal control of connected vehicle systems with communication delay and driver reaction time. IEEE Trans. Intell. Transp. Syst. (2016). doi:10.1109/TITS.2016.2633164
10. Geiger, A., Lauer, M., Moosmann, F., Ranft, B., Rapp, H., Stiller, C., Ziegler, J.: Team Annieway's entry to the 2011 grand cooperative driving challenge. IEEE Trans. Intell. Transp. Syst. **13**(3), 1008–1017 (2012)
11. Happawana, G.S., Nwokah, O.D.I., Bajaj, A.K., Azene, M.: Free and forced response of mistuned linear cyclic systems: a singular perturbation approach. J. Sound Vib. **211**(5), 761–789 (1998)
12. Liu, Z.H., Liu, W., Gao, W.C., Cheng, X.: Advances of research on mode localization in mistuned cyclically periodic structures. Appl. Mech. Mater. **405–408**, 3198–3203 (2013)
13. Lu, X.Y., Hedrick, J.K., Drew, M.: ACC/CACC-control design, stability and robust performance. In: Proceedings of the American Control Conference, vol. 6, pp. 4327–4332. IEEE (2002)
14. Liao, Y., Li, S.E., Wang, W., Wang, Y., Li, G., Cheng, B.: Detection of driver cognitive distraction: a comparison study of stop-controlled intersection and speed-limited highway. IEEE Trans. Intell. Transp. Syst. **17**(6), 1628–1637 (2016)
15. Mangel, T., Michl, M., Klemp, O., Hartenstein, H.: Real-world measurements of non-line-of-sight reception quality for 5.9 GHz IEEE 802.11p at intersections. In: Strang, T., Festag, A., Vinel, A., Mehmood, R., Rico Garcia, C., Röckl, M. (eds.) Communication Technologies for Vehicles, pp. 189–202. Springer, Berlin (2011)
16. Milanés, V., Shladover, S.E.: Modeling cooperative and autonomous adaptive cruise control dynamic responses using experimental data. Transp. Res. Part C Emerg. Technol. **48**, 285–300 (2014)
17. Milanés, V., Shladover, S.E., Spring, J., Nowakowski, C., Kawazoe, H., Nakamura, M.: Cooperative adaptive cruise control in real traffic situations. IEEE Trans. Intell. Transp. Syst. **15**(1), 296–305 (2014)
18. Olson, B.J., Shaw, S.W., Shi, C., Pierre, C., Parker, R.G.: Circulant matrices and their application to vibration analysis. Appl. Mech. Rev. **66**(4), 040803 (2014)
19. Öncü, S., Ploeg, J., van de Wouw, N., Nijmeijer, H.: Cooperative adaptive cruise control: network-aware analysis of string stability. IEEE Trans. Intell. Transp. Syst. **15**(4), 1527–1537 (2014)
20. Orosz, G., Stépán, G.: Subcritical Hopf bifurcations in a car-following model with reaction-time delay. Proc. R. Soc. **462**(2073), 2643–2670 (2006)
21. Orosz, G.: Connected cruise control: modelling, delay effects, and nonlinear behaviour. Veh. Syst. Dyn. **54**(8), 1147–1176 (2016)
22. Pierre, C., Dowell, E.H.: Localization of vibrations by structural irregularity. J. Sound Vib. **114**(3), 549–564 (1987)
23. Ploeg, J., van de Wouw, N., Nijmeijer, H.: Lp string stability of cascaded systems: application to vehicle platooning. IEEE Trans. Control Syst. Technol. **22**(2), 1527–1537 (2014)
24. Qin, W.B., Gomez, M.M., Orosz, G.: Stability and frequency response under stochastic communication delays with applications to connected cruise design. IEEE Trans. Intell. Transp. Syst. **18**(2), 388–403 (2017)
25. Rajamani, R.: Vehicle Dynamics and Control. Springer, Berlin (2011)
26. Roose, D., Szalai, R.: Continuation and bifurcation analysis of delay differential equations. In: Krauskopf, B., Osinga, H.M., Galan-Vioque, J. (eds.) Numerical Continuation Methods for Dynamical Systems, Understanding Complex Systems, pp. 359–399. Springer, Berlin (2007)
27. Shladover, S.E., Nowakowski, C., Lu, X.Y., Ferlis, R.: Cooperative adaptive cruise control (CACC) definitions and operating concepts. In: Proceedings of the 94th Annual TRB Meeting, 15-3265 (2015)
28. Shladover, S.E., Su, D., Lu, X.Y.: Impacts of cooperative adaptive cruise control on freeway traffic flow. Transp. Res. Rec. J. Transp. Res. Board **2324**, 63–70 (2012)
29. Szalai, R., Orosz, G.: Decomposing the dynamics of heterogeneous delayed networks with applications to connected vehicle systems. Phys. Rev. E **88**(4), 040902 (2013)
30. Wei, S.T., Pierre, C.: Localization phenomena in mistuned assemblies with cyclic symmetry part i: free vibrations. J. Vib. Acoust. Stress Reliab. Des. **110**(4), 429–438 (1988)
31. Wang, M., Daamen, W., Hoogendoorn, S.P., van Arem, B.: Cooperative car-following control: distributed algorithm and impact on moving jam features. IEEE Trans. Intell. Transp. Syst. **17**(5), 1459–1471 (2016)
32. Zhang, L., Orosz, G.: Motif-based design for connected vehicle systems in presence of heterogeneous connectivity structures and time delays. IEEE Trans. Intell. Transp. Syst. **17**(6), 1638–1651 (2016)